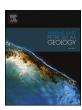
FISEVIER

Contents lists available at ScienceDirect

#### Marine and Petroleum Geology

journal homepage: www.elsevier.com/locate/marpetgeo



#### Research paper

## The Late Pleistocene Po River lowstand wedge in the Adriatic Sea: Controls on architecture variability and sediment partitioning



Claudio Pellegrini<sup>a,\*</sup>, Alessandra Asioli<sup>a</sup>, Kevin M. Bohacs<sup>b</sup>, Tina M. Drexler<sup>c</sup>, Howard R. Feldman<sup>b</sup>, Michael L. Sweet<sup>b</sup>, Vittorio Maselli<sup>d</sup>, Marzia Rovere<sup>a</sup>, Fabiano Gamberi<sup>a</sup>, Giacomo Dalla Valle<sup>a</sup>, Fabio Trincardi<sup>a</sup>

- <sup>a</sup> Istituto di Scienze Marine (ISMAR-CNR), Via Gobetti 101, 40129, Bologna, Italy
- <sup>b</sup> ExxonMobil Upstream Research Company, 22777 Springwoods Village Parkway, Spring, TX 77389, USA
- <sup>c</sup> ExxonMobil Exploration Company, 22777 Springwoods Village Parkway, Spring, TX 77389, USA
- <sup>d</sup> Department of Geology and Petroleum Geology, University of Aberdeen, King's College, Aberdeen, UK

#### ARTICLE INFO

# Keywords: Continental margin evolution Quaternary geology Clinoform Sediment partitioning and prediction Paleoenvironmental reconstruction Sequence stratigraphy Sea level changes Last glacial maximum Climate change effects

#### ABSTRACT

Although facies and stratal geometries of continental margin successions can be defined in detail based on subsurface and outcrop studies, most studies lack the high-resolution age control needed to constrain the time scale of formation of such successions and infer their external forcing mechanisms. Our work on the Po River Lowstand Wedge (PRLW) indicates that deposition rates are surprisingly high with the entire 350-m-thick succession being deposited in less than 17,000 years, and with individual clinothems recording time periods ranging from 400 to 4700 years. The PRLW preserves a high-resolution record of stacked, deltaic shelf-edge clinothems deposited during the Last Glacial Maximum (31.8–14.4 ky BP) in the Adriatic basin (Mediterranean Sea). We investigated clinothem internal geometry, stacking patterns, and facies distributions to infer the main controls on their growth by integrating seismic reflection data with seismic facies attributes and paleoenvironmental proxies. The stratigraphic framework of the shelf-edge clinothems was then related to major paleoenvironmental shifts during the last glacial cycle and driven by eustatic and climatic changes.

Within the PRLW, we recognized three distinctive types of 100's-m-high shelf-edge clinothems, type A, type B and type C, each with diagnostic topset geometries, shelf-edge trajectories, and associated distal basin-fill deposits. These elemental clinothem types stack into two Clinothem Sets. Clinothem Set 1, with essentially flat to slightly descending shelf-edge trajectory, is composed of stacked types A and B clinothems, and records the direct influence of river flux leading to dysoxic conditions on the bottom of the basin. In particular, clinothem accumulation rates were as much as 200 km³/ky in some of the type B clinothems. Clinothem Set 2, showing ascending shelf-edge trajectory, records an aggradational stacking coupled with a retreat of the river-entry points with benthic fauna assemblages that reflect the influence of peaks in freshwater discharge. Whereas Clinothem Set 1 developed under perturbations of river supply linked to the multi-scale waxing and waning of glaciers during an interval dominated by eustatic fall, Clinothem Set 2 reflects the main thawing of glaciers concomitant to the first phase of the eustatic rise. From a sequence stratigraphic perspective, Clinothem Set 1 is interpreted as staked high-frequency sequences, while Clinothem Set 2 represents a stack of high-frequency parasequences.

The high-resolution age control from boreholes and seismic data enabled us to relate stratal character to independently constrained environmental proxies: this revealed how the evolution of a shelf-edge system intricately convolves the influences of both global (eustacy) and regional (climate-driven supply fluctuations) controls, both at sub-Milankovitch scales. Finally, the thickness, geometry, and stacking patterns of the centennial to millennial clinothems of the PRLW vary in systematic ways resulting in geometries that closely resemble those of ancient shelf-edge systems, and offering the PRLW as a sub-modern analogue. Our observations also reinforce the focus of the classic sequence-stratigraphic approach on analyzing surfaces and their geometric relations and not on time duration or formation mechanisms.

E-mail address: claudio.pellegrini@bo.ismar.cnr.it (C. Pellegrini).

<sup>\*</sup> Corresponding author.

#### 1. Introduction

Shelf-margin wedges and associated clinothems are the critical link between continental and deep-water realms and preserve a distinctive record of the growth of continental margins. Although local in extent, on a global scale they have an outsized importance: their strata have been estimated to sequester > 40% of the biogenic carbon in the modern ocean and to host > 40% of global oil reserves, including many important recent discoveries (e.g., Suter and Berryhill, 1985; Walsh, 1991; Sydow et al., 2003; Muller-Karger et al., 2005; IEA, 2013). Detailed analyses of the stratigraphic record in shelf-margin settings can provide useful insights on their response to external and internal forcing mechanisms on time scales longer than available in weather- and oceanographic-instrument records. Therefore the characterization of clinothem evolution within high-resolution chronostratigraphic contexts is a fundamental aid in the reconstruction of continental-margin history and controls (e.g. eustasy and climate), and in the prediction of

hydrocarbon reservoir potential. In this view, sequence stratigraphy is a method through which a systematic analysis of the stratigraphic record can help in reconstructing the evolution of continental margins in time and space (Boyd et al., 1989; Plink-Björklund et al., 2001; Eberli et al., 2002; Johannessen and Steel, 2005; Plint and Kreitner, 2007; Zecchin et al., 2008; Bhattacharya et al., 2016; Hodgson et al., 2018) including the attempt to recognize the allogenic and autogenic stratigraphic responses to unsteady and steady forcing of the external variables (e.g. Muto and Steel, 1997; Jerolmack and Paola, 2010; Madof et al., 2016). Focused initially on million-years time scales (Mitchum et al., 1977), sequence stratigraphy has long since been applied to the study of Quaternary continental margins at Milankovitch-band time scales (mostly at 100,000 year scale). At all scales, accommodation and sediment supply are recognized as the main factors that govern changes in stratal architecture and sediment partitioning across continental margins (e.g. Vail et al., 1977; Boyd et al., 1989; Shanley and McCabe, 1991; Trincardi and Field, 1991; Pillans et al., 1998; Roberts et al.,

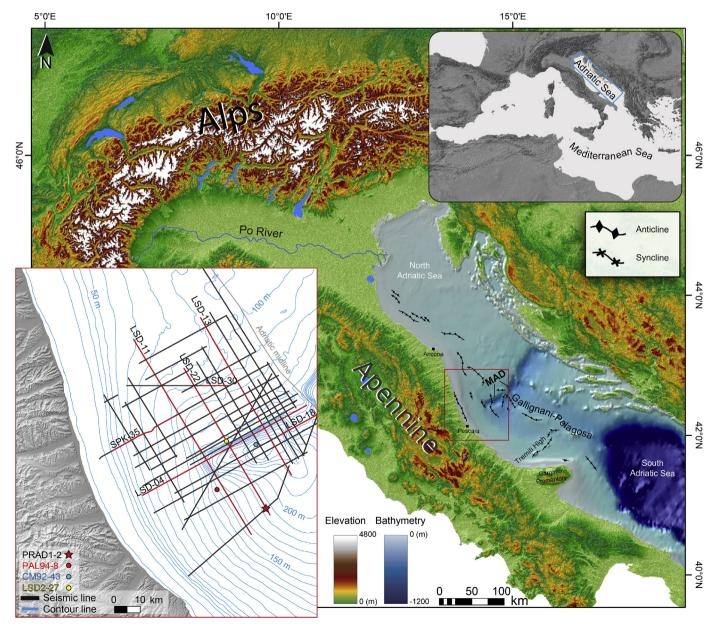


Fig. 1. Digital elevation model for the Adriatic Sea and surrounded area with structural elements. MAD: Mid Adriatic Depression. Top right: Adriatic Sea location in the Mediterranean Sea. Bottom left: detail of the MAD with the location of the seismic grid, sediment cores, and boreholes used in this study. Seismic profiles shown in this paper are highlighted in red. (For interpretation of the references to color in this figure legend, the reader is referred to the Web version of this article.)

2004; Wellner et al., 2004; Fatoke and Bhattacharya, 2010; Anderson et al., 2014, 2016; Klausen et al., 2015; Amorosi et al., 2016; Madof et al., 2017; Embry and Johannessen, 2017).

In the study of continental margins, clinothems have been documented as one of the fundamental building blocks of the stratigraphic record (Asquith, 1970; Helland-Hansen and Martinsen, 1996; Pirmez et al., 1998; Steel et al., 2000; Minisini et al., 2017; Pellegrini et al., 2017a). Clinothems have been recognized over several spatial and temporal scales ranging from shoreline accretion to continental-margin progradation (Vail et al., 1991; Steckler et al., 1999; Swenson et al., 2005; Carvajal et al., 2009; Helland-Hansen and Hampson, 2009; Patruno et al., 2015; Pellegrini et al., 2015) and are sensitive archives of climate and oceanographic regime (e.g. Cattaneo et al., 2003; Swenson et al., 2005; Mallarino et al., 2006; Fanget et al., 2014; Pellegrini et al., 2015; Tesi et al., 2017; Peng et al., 2018).

By studying the anatomy of a 350-m-thick shelf-margin wedge deposited during a single short-lived lowstand of sea level, we document, in a chronologically well-constrained framework (Pellegrini et al., 2017a), a composite succession of late-Pleistocene shelf-edge clinothems recording short-term (sub-Milankovitch scale) environmental and climatic change during the Last Glacial Maximum (LGM). Particular attention has been paid to the characterization of 1) the 3D shape of individual shelf-edge clinothems (100s m thick; up to 5 km of progradation) and their thickness distribution as a function of the Sediment Accumulation Rate (SAR) and accommodation; 2) the vertical and lateral distribution of sedimentary facies, and 3) the timing of and controls on the activity of deep-water channel-lobe complexes.

These results have been combined with a well-constrained suite of paleo-environmental proxies with the aim of testing some of the key concepts typically adopted in the reconstructions of recent and ancient progradational margins. We thus are able to correlate our observations on clinothem development with a suite of environmental parameters to link stratigraphic variations to their possible causes. The main goal of this paper is to illustrate how the growth of this shelf-margin wedge was controlled by the intricate interactions of climatic variations and eustatic oscillations that effected sediment-supply fluctuations and the character of sedimentation in the different sectors of a prograding margin. Finally, we highlight the role of sub-Milankovitch cyclicity in controlling the stacking pattern of clinothems and clinothem sets even down to centennial-to millennial-scale variations in the rates of sediment supply and fresh-water discharge and accompanying environmental changes.

#### 2. Setting

#### 2.1. Geological evolution of the adriatic foredeep

Following the early Alpine compression that led to the closure of the Tethys in the late Cretaceous (Doglioni et al., 1994), the Mediterranean region was characterized by a compressive regime affecting the Apennine mountain chain starting in the Oligocene. During the lower Pliocene, the eastward migration of the Apennine front induced the tilting of the Adriatic foreland toward the orogenic front, causing the formation of foredeep depocenters of variable-thickness and their subsequent infill through Quaternary prograding successions along the axis of the basin (Royden et al., 1987; Dalla Valle et al., 2013; Ghielmi et al., 2013; Rossi et al., 2015).

In the north-central Adriatic basin, the most recent southeastward prograding successions (Fig. 1), is of late Pleistocene age (Trincardi et al., 1994). The late Pleistocene succession encompasses the eustatic lowstand of the Last Glacial Maximum (LGM; Fig. 2), when the Po River Lowstand Wedge (PRLW) recorded a 40 km shelf-edge progradation (Pellegrini et al., 2017a, Fig. 3) partially filling the Mid Adriatic Dip (MAD), a remnant slope basin that was ca. 450 m deep (Pellegrini et al., 2017b). During the deposition of the PRLW, most of the underlying tectonic structures were inactive (Fig. 4); however, some active

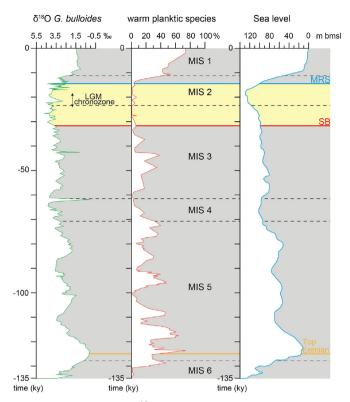


Fig. 2. Plot of foraminiferal  $\delta^{18}$ O (*G. bulloides*), warm planktic species (from Piva et al., 2008a, b; see Data, Material and Strategy for the species included), and eustatic curve (Chappell and Shackleton, 1986). Vertical scale is in time (ky BP). Horizontal dashed lines mark the boundaries of Marine Isotopic Stages. The PRLW forms between SB and MRS surfaces (yellow interval), during an overall cold climatic interval and encompasses the late phase of eustatic fall, the lowstand, and the early phase of eustatic rise. (For interpretation of the references to color in this figure legend, the reader is referred to the Web version of this article.)

structures, possibly related to halo-kinetic deformation of Triassic evaporates, punctuate the eastern sector of the MAD (Geletti et al., 2008).

### 2.2. Adriatic basin physiography from the last interglacial through Last Glacial Maximum times

During the last previous interglacial (Marine Isotope Stage 5e, MIS 5e, ~132-116 ky BP, Bazin et al., 2013) the physiography of the Adriatic basin was similar to the modern one, with a shoreline somewhat landward of the modern position (Amorosi et al., 2004). The ensuing step-wise lowering of sea level between oxygen-isotope Substage 5e and the Marine Isotope Stage 2 (ca. ~132-116 to 11.7 ky BP, Walker et al., 2009; Bazin et al., 2013, Fig. 2), promoted a marked basinward shift of the shoreline and the formation of a regionally-extensive unconformity associated with alluvial-plain sedimentation in the northern, shallower reaches of the basin (Amorosi et al., 2016). From land to basin, the succession of MIS 3 and MIS 2 is identified as: 1) paleosols and associated channel-belt deposits in the northern and southern Adriatic coastal plain (Amorosi et al., 2017; Bruno et al., 2017; Campo et al., 2017); 2) an extensive hiatal surface across a significant portion of the area presently occupied by the modern shelf (Amorosi et al., 2016); and 3) a thick sedimentary succession that fills in the MAD (Fig. 3), recording glacio-eustatic oscillations at Milankovitch and sub-Milankovitch scales (Piva et al., 2008a; Pellegrini et al., 2017a). In essence, the interval between the MIS 5e and the onset of the LGM (at ca. 26 ky BP) spanned a substantial shrinking of the Adriatic basin and the concurrent broadening of the Po plain drainage area with a stepwise

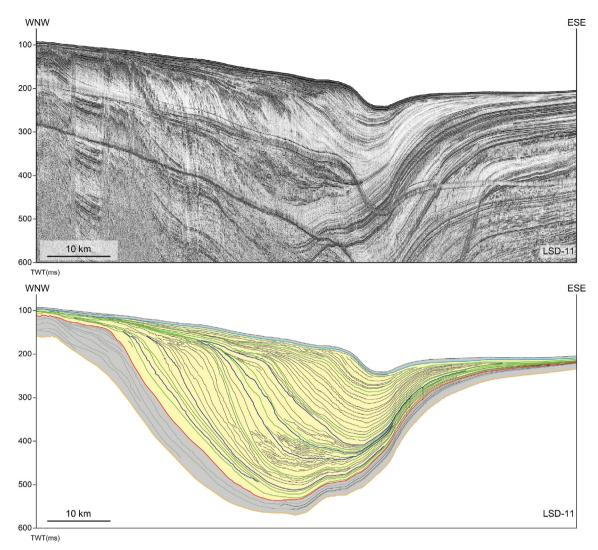


Fig. 3. Line drawing of LSD-11 multichannel profile showing the late Pleistocene Po River Lowstand Wedge (PRLW) in yellow. Note that the PRLW comprises clinothems with continual bottomset aggradation. (For interpretation of the references to color in this figure legend, the reader is referred to the Web version of this article.)

displacement of the shoreline up to ca. 250 km southeastward (Amorosi et al., 2016), and a relative position of sea level at ca. 130 m lower than present day (e.g. Lambeck et al., 2014; Benjamin et al., 2017). During that time interval, extensive glaciers capped the Alpine chain (Florineth and Schluchter, 1998; Monegato et al., 2007, 2017) nourishing the ancestral Po River system which debouched into the central Adriatic slope basin promoting the formation of the PRLW during overall cold climatic conditions (Fig. 2; Pellegrini et al., 2017a).

#### $2.3. \ \ \textit{Sediment supply: modern and inferred for the Last Glacial Maximum}$

The modern Adriatic basin is fed mainly by Alpine and Apennine Rivers. Sediment yield from the Dinarides to the east is negligible because of the intensely fractured and karstic nature of the catchments that trap water and sediment influx in basins close to the coastal area (Simeoni et al., 1997; Milliman and Farnsworth, 2013; Milliman et al., 2016). Fluvial sediment sources along the western side of the Adriatic Basin form a "line source", with combined modern delivery of  $51.7 \times 10^6$  tons yr $^{-1}$  of mean suspended load and an average freshwater discharges of  $1500~{\rm m}^3~{\rm s}^{-1}$  (Frignani et al., 2005; Cattaneo et al., 2003). In contrast, during the LGM the drainage system of the ancestral Po River was more than double its current size, reaching about  $190,000~{\rm km}^2$ , compared to the modern catchment of  $94,000~{\rm km}^2$ 

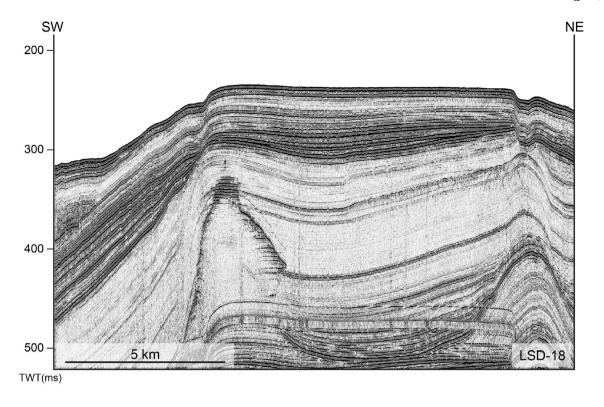
(Kettner and Syvitski, 2008). The average suspended sediment flux into the Northern Adriatic Sea during the Pleistocene is estimated to have been  $46.6\times10^6$  tons yr $^{-1}$ , with an average freshwater discharge of  $3000~\text{m}^3~\text{s}^{-1}$ ; from the Po River alone (Kettner and Syvitski, 2008).

#### 3. Data, methods, and strategy

#### 3.1. Seismic data, borehole and sediment cores

The main set of reflection-seismic profiles used for this work was acquired during the LowStand Delta (LSD) 2014 cruise and was shot using a mini water-gun source (Sercel S15-02 of 15 inc³) and recorded through a multichannel streamer (Teledyne mini-streamer with 24 channels; 80–500 Hz frequency band width). These data were complemented by single-channel profiles shot with a 300-J Sparker electromechanic source and by a dense grid of CHIRP sub-bottom lines with a 2–7 kHz outgoing signal. All data were digitally recorded after bandpass filtering and gain adjustment. The seismic grid comprises high-resolution seismic profiles with a total length of 1500 km and covers an area of 5000 km² centered in the MAD (Fig. 1). In addition, a multibeam bathymetry of the MAD was acquired using a Kongsberg EM710 hull-mounted multibeam and gridded at 20 m resolution.

The seismic grid has been tied to the PRAD1-2 borehole (Pellegrini



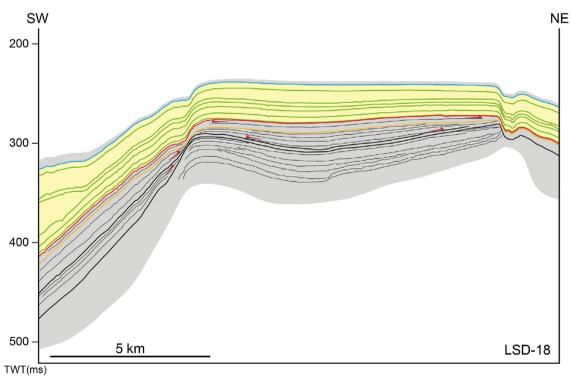


Fig. 4. Multichannel LSD-18 line drawing shows stratal terminations indicating that tectonic activity was quiescent during the PRLW accumulation (yellow interval). (For interpretation of the references to color in this figure legend, the reader is referred to the Web version of this article.)

et al., 2017a), a 71.2 m long borehole with a total recovery of 99.6% sampled in 185.5 m water depth (Fig. 1). Seismic-stratigraphic correlation from the expanded stratigraphic clinoform succession to the distal borehole is straightforward, and was corroborated for the upper ca. 80 m of the succession by correlation through a network of CHIRP profiles. Key stratigraphic surfaces of regional extent are tied to PRAD1-2 borehole with a vertical resolution of 0.3–0.5 m (Fig. 5).

The PRAD1-2 borehole and two other sediment cores were analyzed in detail for microfossils to form a composite biostratigraphic section. Sediment core CM92-43 is located at 252 m water depth at the bottom of the slope, and sediment core PAL94-8 is at 150 m water depth close to the shelf-edge (Trincardi et al., 1996). The chronology of these two cores, already published by Asioli (1996) and Asioli et al. (2001), is here partially revised for the interval older than 15 ky BP (Table 1; see

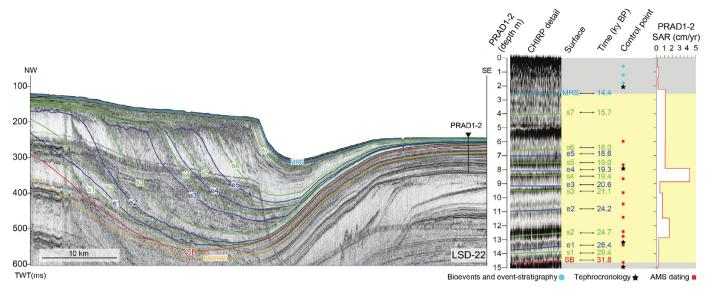
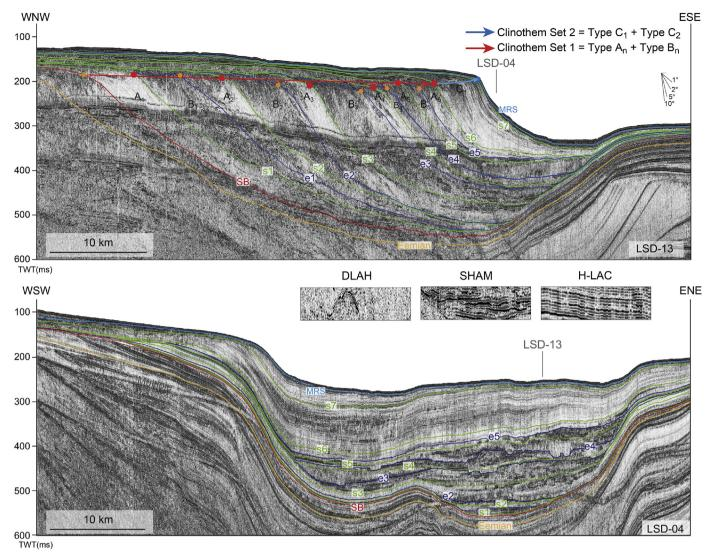


Fig. 5. Dip-oriented multichannel seismic profile LSD-22 illustrates clinothem geometry along the main direction of progradation. Orange horizon marks top of Eemian (ca. 125 ky B.P.); red horizon is sequence boundary (SB) at base of PRLW; green horizons (s) mark surfaces on top of type A and type C clinothems whereas blue horizons (e) are on top of type B clinothems; light blue horizon is maximum regression surface (MRS) on top of younger C<sub>2</sub> clinothem (clinothems are numbered from older to younger). Seismic horizons are tied to PRAD1-2 borehole through high-resolution CHIRP sonar profiles. The 16 control points and the name and age of seismic horizons are reported along the 15 m succession. SAR (sediment accumulation rate) is given in cm/yr. (For interpretation of the references to color in this figure legend, the reader is referred to the Web version of this article.)

Table 1
The age model for the PRLW succession based on PRAD1-2 borehole, PAL94-8 and CM92-43 sediment cores (see supplemental material) and incorporating <sup>14</sup>C dates, tephra layers, bio and stratigraphic events.

Sample top (m)	Control points	Source	Reference	Status
PRAD1-2				
0	0	modern time	Pellegrini et al. (2017a,b)	
0.6	6000	LO G. inflata	Pellegrini et al. (2017a,b)	
1.288	8500	Sapropel equivalent 1	Pellegrini et al. (2017a,b)	
1.8	12000	Top GS-1	Pellegrini et al. (2017a,b)	
2.18	14110	Neapolitan Yellow Tuff	Pellegrini et al. (2017a,b)	
5.976	17540	<sup>14</sup> C	Pellegrini et al. (2017a,b)	
7.82	19275	<sup>14</sup> C + Greenish/Verdoline	Pellegrini et al. (2017a,b)	
8.8	19498	<sup>14</sup> C	Pellegrini et al. (2017a,b)	
9.6	21350	<sup>14</sup> C	Pellegrini et al. (2017a,b)	
10.50	22528	<sup>14</sup> C	Pellegrini et al. (2017a,b)	
11.40	23780	<sup>14</sup> C	Pellegrini et al. (2017a,b)	
12.78	24725	<sup>14</sup> C	Pellegrini et al. (2017a,b)	
13.36	27200	VRa + <sup>14</sup> C	Pellegrini et al. (2017a,b)	
14.8	32350	<sup>14</sup> C	Pellegrini et al. (2017a,b)	
14.94	33300	Codola (base)	Pellegrini et al. (2017a,b)	
16.53	39500	Campanian Ignimbrite	Pellegrini et al. (2017a,b)	
PAL94-8				
1.78-1.82	8631-9074	<sup>14</sup> C	Asioli (1996)	accepted
2.05	11500	Top GS	Asioli et al. (2001)	accepted
2.08	14110	Neapolitan Yellow Tuff	Calanchi and Dinelli (2008)	rejected
2.28-2.32	13350-13742	14C	Asioli (1996)	rejected
2.40-2.41	14653	Abrupt increase of G. ruber at base of GI-1	Asioli (1996); Asioli et al. (2001)	accepted
3.53-3.54	16002 (interpolated)	Y1 tephra	Calanchi and Dinelli (2008)	accepted
4.64-4.68	17169–17695	<sup>14</sup> C	Asioli (1996)	accepted
CM92-43				•
3.90	10480	<sup>14</sup> C	Asioli et al. (2001)	accepted
3.98	11390	<sup>14</sup> C	Asioli et al. (2001)	accepted
1.33	11750	<sup>14</sup> C	Asioli et al. (2001)	accepted
4.53	12005	<sup>14</sup> C	Asioli et al. (2001)	accepted
4.93	12700	<sup>14</sup> C	Asioli et al. (2001)	accepted
5.05	14110	Neapolitan Yellow Tuff	(Bourne et al., 2010)	accepted
6.50	14653	Abrupt increase of <i>G. ruber</i> at base of GI-1	Asioli et al. (2001)	accepted
5.80	14900	δ <sup>18</sup> O stratigraphy TI A	Asioli et al. (2001)	accepted
10.48	16002	(from core Pal94-8)	this study	accepted



**Fig. 6.** Top: Dip-oriented multichannel seismic profile LSD-13 illustrating clinothem geometries along the main direction of progradation. Bottom: Along-strike profile LSD-04 highlighting the seismic facies of basinal deposits (see Fig. 1 for seismic lines location). Orange horizon marks top of Eemian (ca. 125 ky BP); red horizon is Sequence Boundary (SB) at base of PRLW; green horizons (s) mark surfaces on top of type A and type C clinothems whereas blue horizons (e) are on top of type B clinothems; light blue horizon is the Maximum Regression Surface (MRS) on top of youngest C<sub>2</sub> clinothem (clinothems are numbered from older to younger). Red, orange, and blue dots mark shelf-edge of type A, B, and C clinothems, respectively. Surface s6 marks transition from progradational Clinothem Set 1 (comprising stacked type A and B clinothems) to aggradational Clinothem Set 2 (constituted by stacked type C clinothems). Insets illustrate distal basin seismic facies associated with type A (Discontinuous and Low-Amplitude reflections with internal Hyperbolic diffractions, DLAH), type B (Semi-continuous, High-Amplitude and Mounded reflections, SHAM) and type C clinothems (High- and Low-Amplitude Continuous reflections, H-LAC) in basin. (For interpretation of the references to color in this figure legend, the reader is referred to the Web version of this article.)

supplemental material). The sediment core LSD2-27 at 146 m water depth has been sedimentologically analyzed to characterize lithology at the outer shelf.

#### 3.2. Seismic interpretation and analysis

We conducted seismic-stratigraphic interpretation and then seismic-facies analyses to delineate genetically related strata and infer depositional conditions. The interpretation of seismic profiles was based on the principles of seismic stratigraphy (Mitchum et al., 1977; Mitchum and Van Wagoner, 1991), and the accommodation-succession method (Neal and Abreu, 2009; Neal et al., 2016). Following these approaches, which use reflection terminations as the principal criteria for the recognition of seismic sequence boundaries, the Sequence Boundary (SB) at the base of the PRLW was identified on the shelf by toplap and onlap terminations of respectively the underlying and overlying reflections (angular unconformity of Mitchum et al., 1977), and traced basinward

to a correlative conformity with widespread onlap and downlap terminations of the overlying reflections (Figs. 6 and 7; Pellegrini et al., 2017b). The Maximum Regression Surfaces (MRS), atop the PRLW, separates progradational-aggradational stacking from retrogradational stacking of coastal transgressive strata on the shelf (see Pellegrini et al., 2017a) and corresponds with a marine onlap surface of limited extent on the slope (according to the definition by Catuneanu et al., 2009).

Within the PRLW, we recognized three types of shelf-edge clinothems based on topset geometry, shelf-edge- and onlap-point-trajectory, and internal seismic facies (Pellegrini et al., 2017a). Seismic-facies analysis is the description, mapping, and geologic interpretation of seismic-reflection parameters within a chronostratigraphic framework of sequence boundaries (after Mitchum et al., 1977). We delineated the external form, internal reflection characteristics, and 3-D associations of the stratal units within the larger seismic-stratigraphic framework to assure the identification and correlation of genetically related strata. Reflection configuration reveals gross stratification patterns from which

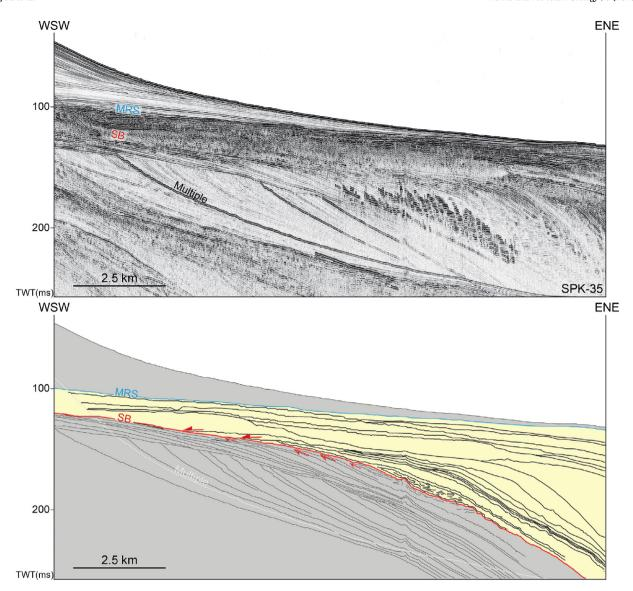


Fig. 7. Detail of the line drawing of SPK-35 sparker profile (along-strike orientation). Seismic terminations highlight the SB at base of the PRLW with coastal onlap docked close to the shelf-edge (after Pellegrini et al., 2017b).

depositional processes and erosion can be interpreted (e.g. Pellegrini et al., 2016). Reflection continuity is closely associated with continuity of strata; continuous reflections suggest widespread, uniformly stratified deposits. Reflection amplitude contains information on the velocity and density contrasts of individual bedding interfaces and their spacing. It is used to predict lateral bedding changes. Reflection spacing ('frequency'), although mainly a characteristic of the seismic pulse, is also related to such geologic factors such as the spacing of reflectors and lateral changes in interval velocity (due to lithofacies and pore-fluid changes). Grouping these seismic parameters into mappable seismicfacies facilitates their interpretation in terms of lithotype, depositional processes and environment, possible sediment entry-point locations, and geological setting. Within the PRLW distinctive seismic facies are grouped into 11 generic subclasses (Table 2). The criteria we used to distinguish different facies included seismic-reflection amplitude, continuity, and dip (where dipping reflections are  $> 0.8^{\circ}$ ), internal reflection character, and the nature of their boundaries, as well as their position in the depositional system (Table 2 and Fig. 6).

Trajectory analysis considers lateral and vertical migration of geomorphological features and associated sedimentary environments, with emphasis on the paths and direction of migration of the coastal onlap points and correlative shelf edges (Steel et al., 2000; Henriksen et al.,

2009 and reference there in). We conducted shelf-edge trajectory analysis in due consideration of the fact that the rollover point (offlap break of Vail et al., 1977 and Jervey, 1988) at the topset-foreset transition of a clinothem can occur in shelfal marine environments and thus might not necessarily represent the shoreline (i.e., the shelf-edge rollover point, at best, only approximates the shoreline position: see Pellegrini et al., 2015 and discussion therein). Key stratigraphic surfaces of regional extent and seismic facies (Table 2) were recognized, correlated, looptied, and mapped using Petrel\* software. The maps of these key stratigraphic surfaces were constructed by using a "convergent interpolation" method. A seismic velocity of 1600 m/s, as suggested by the soniclog analyses (Maselli et al., 2010), was adopted to convert two-way travel times (TWTT) into depth units and to calculate the volume of seismic units.

The nature of the key surfaces and the reflection configurations of the clinothems were then combined with the timing of their formation to examine the relative roles of controlling factors on deposition and sediment distribution such as eustasy and sediment supply. For each clinothem, the progradation and the Sediment Accumulation Rate (SAR) are given as horizontal migration and vertical thickness, respectively, at the corresponding shelf-edge divided by their time duration.

Table 2
Seismic facies template for the PRLW explaining the acronyms and the color legend used in the main text and in the seismic facies maps. A summarized seismic facies description and interpretation is also reported.

Seismic facies	Acronym and color in seismic facies map	Internal Reflections	Clinoform sector	Depositional Environment
100 m 5 ms	HAC	High Amplitude Continuous	Topset	Delta plain/ subaqueous shelf
100 m	HACh	High Amplitude Chaotic	Topset/ Foreset	Delta/Coastal plain
100 m (20 ) 5 ms	HAD	High Amplitude Discontinuous	Topset	Lagoon
. <u>200 m</u> 10 ms	LACDip	Low Amplitude Continuous Dipping	Foreset	Prodelta
200 m 10 ms	HACDip	High Amplitude Continuous Dipping	Foreset	Prodelta
200 m 10 ms	HAChDip	High Amplitude Chaotic Dipping	Foreset	Prodelta
200 m 5 ms	HACWDip	High Amplitude Continuous Wavy Dipping	Foreset	Prodelta
<u>200 m</u> 5 ms	DLAH	Discontinuous Low Amplitude Hyperbolic	Foreset/ Bottomset	Mass-Transport Complexes
500 m 10 ms	SHAM	Semi-continuous High Amplitude Mounded	Foreset/ Bottomset	Channel-levee Complexes
<u>500 m</u> 5 ms	LAC	Low Amplitude Continuous	Bottomset	Distal Basin
500 m 10 ms	HAC	High Amplitude Continuous	Bottomset	Distal Basin

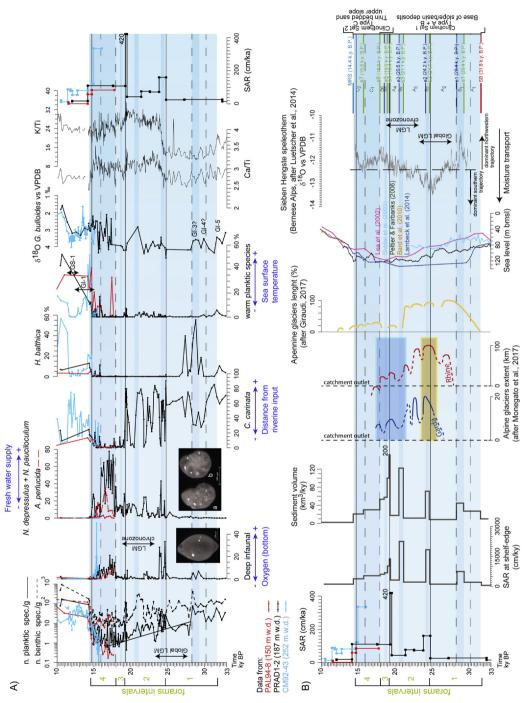


Fig. 8. A) Planktic and benthic foraminifera records of the cores CM92-43 (blue curves) and Pal94-8 (red curves) and of the borehole PRAD1-2 (black curves) plotted vs age. Note that the foraminifera concentration is banner represents major culminations and pale-blue banner ice decay) of the Garda and Rhine glaciers relative to the catchment outlet (dashed line; from Monegato et al., 2017), and of the Apennine glaciers (from Giraudi, 2017), and Bernese Alps speleothem record. Time span by foraminifera intervals and type of clinothems are outlined for comparison. (For interpretation of the references to color in this figure legend, the reader is B) Planktic and benthic foraminifera records along with eustatic curves, Sediment Accumulation Rate (SAR) from PRAD1-2 borehole and measured at the shelf-edge, clinothem volumes, curves of advance/retreat (yellow plotted on logarithmic scale. The intervals corresponding to the Global LGM and to the LGM Chronozone are also reported. GI-1 = Greenland Interstadial 1 (Bolling/Allerod), GS-1 = Greenland Stadial 1 (Younger Dryas); referred to the Web version of this article.)

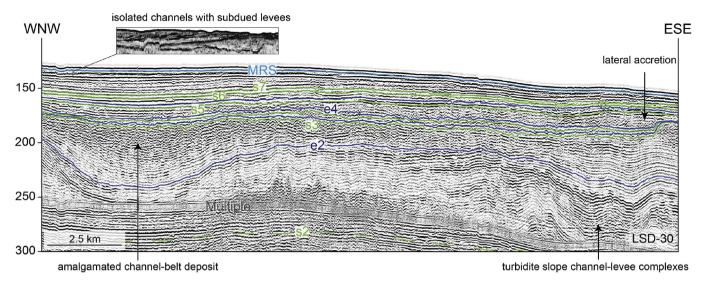


Fig. 9. Detail of LSD-30 multichannel profile with along strike orientation. Note the decreasing dimensions of feeder systems and valley-related features and seismic unit thickness from the bottom to the top of the succession. The stratigraphic surface (s2) below the multiple is represented by a dotted line. Between s2 and e2 surfaces, sediment strata up to several tens of meters thick show parallel to wedge-shaped, high-amplitude reflection packages that pass laterally to low-amplitude reflections reminiscent of turbidite channel-levee complexes in the foreset (e.g. B<sub>2</sub> clinothem); between e2 and s3, seismic facies suggest the presence of amalgamated channel-belt deposits (e.g. A<sub>3</sub> clinothem); between e4 and s5, seismic facies and reflection terminations suggest the presence of isolated incised valleys with internal point-bar migration (e.g. A<sub>5</sub> clinothem); between s7 and MRS, seismic facies and reflection geometries highlight isolated channels with subdued levees (e.g. C<sub>2</sub> clinothem; detail of CHIRP profile).

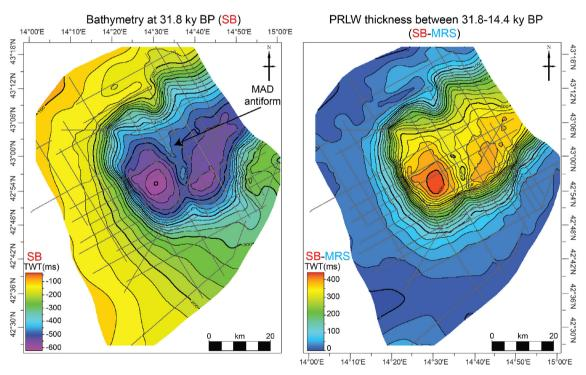


Fig. 10. Structural map of SB surface at 31.8 ky BP and the thickness map of the PRLW. Darkest color represents the deepest and thinner sector. (For interpretation of the references to color in this figure legend, the reader is referred to the Web version of this article.)

#### 3.3. Analyses of micropaleontology

Planktic and benthic foraminifera concentrations are expressed as number of specimens per gram of dry sediment, whereas the species are expressed as percentages. *Globigerinoides sacculifer* includes

Globigerinoides trilobus, Globigerinoides quadrilobatus and Globigerinoides sacculifer according to Hemleben et al. (1989). The category "warm planktic species" in Fig. 8 includes species that preferred warm waters, such as Globigerinoides ruber, Globoturborotalita rubescens, Globigerinoides tenellus, G. sacculifer, Globigerinella praecalida, Orbulina universa (Pujol

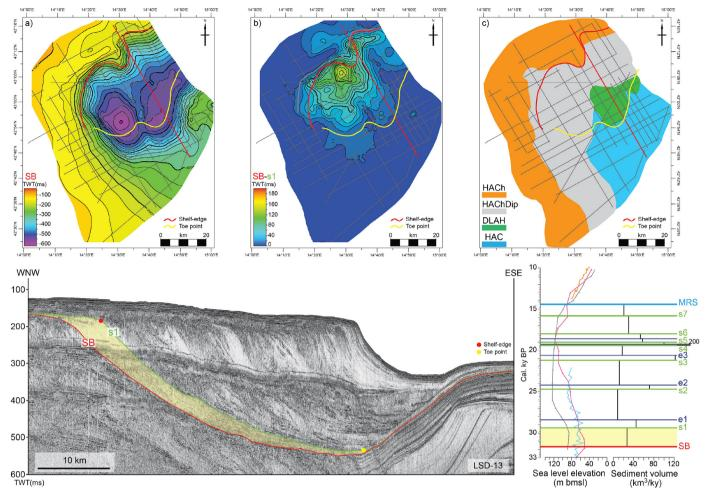


Fig. 11. Clinothem  $A_1$ . Top: a) structural map; b) thickness map; c) seismic facies map (see Table 2 for color legend). Bottom: LSD-13 multichannel profile, eustatic curves (purple curve: Lea et al., 2002; light blue: Siddall et al., 2003; black curve: Peltier and Fairbanks, 2006; yellow curve: Bard et al., 2010; blue curve: Lambeck et al., 2014) and sediment volume (km³/ky) are given for each clinothem that constitute the PRLW. (For interpretation of the references to color in this figure legend, the reader is referred to the Web version of this article.)

#### and Vergnaud-Grazzini, 1995).

Among the benthic foraminifera, the "deep-infaunal" group mainly comprises the benthic species *Glandulina laevigata* and, occasionally, by *Fursenkoina*, a taxon adapted to a deep infaunal microhabitat and especially resistant to low-oxygen conditions (Jorissen et al., 1993, 1999). *Glandulina laevigata* is reported as very rare in biocenosis restricted to Arctic (Knudsen, 1971; Murray, 2013), Atlantic and Indian oceans with highest abundances in slightly hypersaline Arabian Gulf shelf (Murray, 2013). Here we tentatively include this taxon in the deep-infaunal community on the basis of its great morphological affinity with the taxa, including *Glandulonodosariidae*, that went extinct during the Last Global Extinction (Pliocene-Mid Pleistocene Transition, see Hayward et al., 2012 for more details), whose habitat was infaunal with enhanced food supply and consequent low oxygen concentrations, as suggested by geochemical analyses ( $\delta^{13}$ C).

#### 3.4. Age control

The age span of the clinothems of the PRLW was derived from the

chronology of the borehole PRAD1-2 analyzed in detail by Pellegrini et al. (2017a) for the time interval MIS 3-MIS 2, with 106 samples counted for foraminiferal content through a ca. 16.5 m thick succession (regarding the sample preparation and the counting method the reader is referred to Piva et al., 2008a). The age-model relies on a quantitative assessment of the variations in relative abundance of the diverse foraminifera species, stable isotope records, <sup>14</sup>C AMS dates, and tephrochronology on macro and cryptotephra (Bourne et al., 2010), as well as on bioevents and event-stratigraphy (Fig. 5 and Table 1).

#### 4. Results

#### 4.1. Chronology of the PRLW

The base (SB) and the top (MRS) of the PRLW intersect the PRAD1-2 borehole at 14.6 m (bmsl) and 2.5 m (bmsl), respectively, bracketing the entire PRLW between 31.8 cal. ky BP and 14.4 cal. ky BP (Fig. 5; Pellegrini et al., 2017a). The chronological data indicate therefore that the PRLW represents an expanded stratigraphic succession up to 350-m

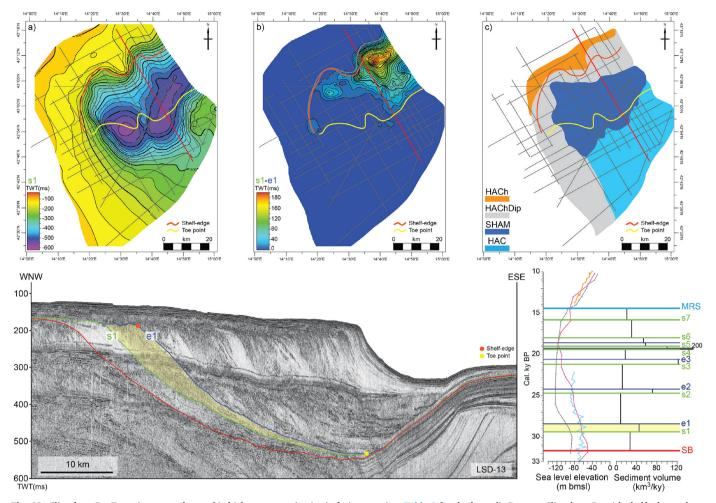


Fig. 12. Clinothem  $B_1$ . Top: a) structural map; b) thickness map; c) seismic facies map (see Table 2 for the legend). Bottom: Clinothem  $B_1$  with shelf-edge and toe points (orange and yellow dot, respectively). The time spanned by Clinothem  $B_1$  along with sediment volume (km $^3$ /ky) and eustatic curves are highlighted in yellow. For references of eustatic curves see Fig. 11 caption. (For interpretation of the references to color in this figure legend, the reader is referred to the Web version of this article.)

thick that developed in only ca. 17 ky during the latest phase of eustatic fall, the LGM eustatic lowstand, and the early phase of eustatic rise (Figs. 2 and 5). Between the SB and MRS, the key stratigraphic surfaces were mapped across the seismic grid and tied to the PRAD 1-2 borehole to estimate their chronological ages.

#### 4.2. Micropaleontology 31.8-14.6 ky

Due to favorable conditions of accommodation and sediment supply, middle Pleistocene regressive successions are exceptionally expanded in the Central Adriatic (Trincardi and Correggiari, 2000; Ridente et al., 2009), and the MIS 5e-MIS 2 interval (late Pleistocene), in particular, preserves a nearly continuous record of a 100-ky-order stepwise fall of sea level (Ridente et al., 2009). Starting from the SB at 31.8 ky BP the PRLW succession shows four intervals that are characterized by distinct foraminifera assemblages (Fig. 8):

**Interval 1** (31.8–24.7 ky BP: clinothems A<sub>1</sub> to A<sub>2</sub>; Fig. 8). Both planktic and benthic foraminifera are present, although planktic

foraminifera are more scarce (up to one order of magnitude in some intervals). The planktic assemblage is largely dominated by *Turborotalita quinqueloba* and occasionally by *Globigerina bulloides*. At 28.2 ky BP (corresponding ca. to e1 surface), the concentration of planktic foraminifera shows an abrupt decrease. The benthic assemblage is largely dominated by *Cassidulina carinata*, except during the pronounced inflection between 30.2 and 28.2 ky BP, where *C. carinata* is replaced by miliolids and later by *Hyalinea balthica*. Deep infaunal taxa are rare and below 10% of abundance.

**Interval 2** (24.7–19.2 ky BP: clinothems  $B_2$  to  $A_5$ ; Fig. 8). Planktic-foraminifera abundance and benthic concentration show an upward decreasing trend, starting from 21 ky (close to  $A_3$ - $B_3$  clinothem boundary). This interval is characterized by closely spaced fluctuations in the abundance of *C. carinata* and includes the continuous occurrence of *Nonion depressulus* and *Nonion pauciloculum*, whereas deep infaunal taxa peak only at the base of the interval. The planktic assemblage is similar to the previous Interval 1.

Interval 3 (19.2-18.0 ky BP: clinothems  $B_5$  to  $A_6$ ; Fig. 8). The

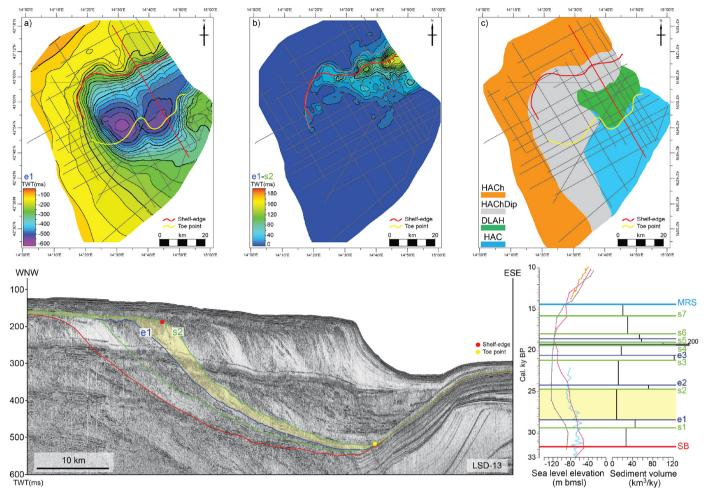


Fig. 13. Clinothem  $A_2$ . Top: a) structural map; b) thickness map; c) seismic facies map (see Table 2 for the legend). Bottom: Clinothem  $A_2$  with shelf-edge and toe points (red and yellow dot, respectively). The time spanned by Clinothem  $A_2$  along with sediment volume (km $^3$ /ky) and eustatic curves are highlighted in yellow. For references of eustatic curves see Fig. 11 caption. (For interpretation of the references to color in this figure legend, the reader is referred to the Web version of this article.)

concentration of both planktic and benthic foraminifera decrease further and the *C. carinata* abundance drops to zero. *N. pauciloculum* and *N. depressulus* show abundances similar to the previous interval, as well as deep infaunal taxa, always present although with low frequency.

**Interval 4** (18.0–14.6 ky BP: clinothems  $C_1$  to  $C_2$ ; Fig. 8). During this interval the concentration of planktic and benthic foraminifera reaches a minimum compared to the rest of the PRLW, and the planktic component drops close to zero (2 specimens per gram on average, mainly belonging to *T. quinqueloba*). *N. pauciloculum* and *N. depressulus* make up to the 80% of the foraminifera assemblage. This turnover of the benthic assemblage is accompanied by a marked increase of deep infaunal taxa.

#### 4.3. Seismic facies description and inferred depositional environments

The most striking feature seen on dip-oriented seismic lines are the hundred-meter-thick clinothems that dip southward (Figs. 3 and 6). The internal architecture of these clinothems changes giving a repeated common suite of seismic facies that have been interpreted as clues to

the sedimentary processes that shaped the clinothems.

#### 4.3.1. Topset seismic facies (HAC, HACh, HAD)

The topsets of all three types of clinothems are characterized by High Amplitude Continuous reflectors (HAC) that change laterally to High Amplitude Chaotic reflectors (HACh). The latter are discontinuous, irregular reflections (Table 2). At the modern seafloor, High Amplitude Discontinuous reflections (HAD) characterize deposits with irregular spatial distribution.

#### 4.3.2. Topset inferred depositional environment

The topset seismic facies are interpreted as coastal-plain deposits: HAC are interpreted as delta plain sandy-silty deposits that change laterally to HACh reflections interpreted as amalgamated fluvial channel belts with sandy-muddy fill (Table 2). At the modern seafloor, HAD reflections characterize lagoon deposits formed behind highly discontinuous and reworked barrier features with sparse distribution as documented by earlier publications (Trincardi et al., 1994; Storms et al., 2008).

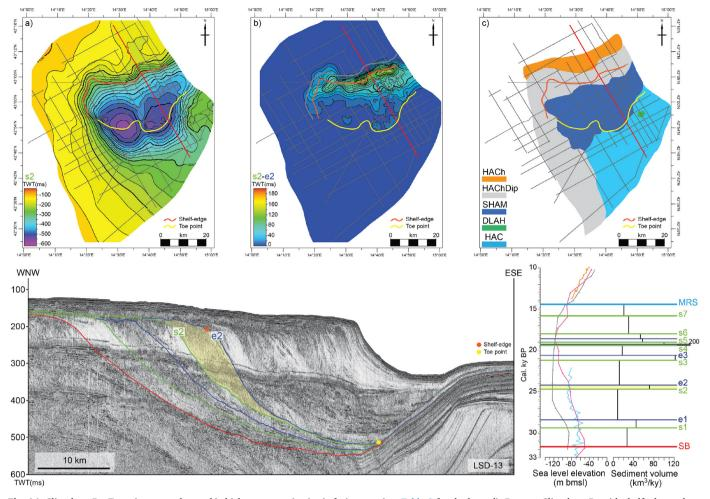


Fig. 14. Clinothem  $B_2$ . Top: a) structural map; b) thickness map; c) seismic facies map (see Table 2 for the legend). Bottom: Clinothem  $B_2$  with shelf-edge and toe points (orange and yellow dot, respectively). The time spanned by Clinothem  $B_2$  along with sediment volume (km $^3$ /ky) and eustatic curves are highlighted in yellow. For references of eustatic curves see Fig. 11 caption. (For interpretation of the references to color in this figure legend, the reader is referred to the Web version of this article.)

#### ${\it 4.3.3. Upper foreset seismic facies (HAChDip-HACDip-HACWDip-LACDip)}$

Foresets are characterized by a variety of seismic facies: High Amplitude Chaotic Dipping reflections (HAChDip), High Amplitude Continuous Dipping reflections (HACDip) and Low Amplitude Continuous Dipping reflections (LACDip) are present in the topset-foreset transition sector of clinothems. Locally, parallel to wedge-shaped high-amplitude reflection packages pass laterally to low-amplitude reflections that characterize strata up to several tens of meters thick (Fig. 9). In addition, packages up to 10-m-thick composed of High Amplitude Continuous Wavy and Dipping reflections (HACWDip; Table 2), characterize the clinothems developed in the western sector of the MAD.

#### 4.3.4. Upper foreset inferred depositional environment

Located seaward from the coastal-plain and channel-belt deposits, HAChDip reflections suggest the presence of distributary channels that extended over the shelf-edge and into upper slope (Table 2). The HACDip and LACDip reflections are interpreted as heterolithic foreset deposits, related to the delta front and prodelta-slope zone. Locally,

wedge-shaped reflections indicate the presence of channel-levee systems several tens of meters thick acting as a major conduits of sediment bypass from the shelf to the basin (Fig. 9). The HACWDip reflections include 10-m-scale crenulated features resembling those documented on several late-Holocene prodelta deposits (see Urgeles et al., 2011 and references therein).

#### 4.3.5. Lower foreset-bottomset seismic facies (SHAM-DLAH-HLAC)

Three characteristic seismic facies developed in the transitional area between foreset and bottomset. Semi-Continuous High Amplitude Mounded reflections (SHAM), Discontinuous Low Amplitude reflections with internal Hyperbolic diffractions (DLAH), and High- and Low-Amplitude Continuous reflections (HLAC). The first two seismic facies characterize clinothems developed during the first phases of PRLW progradation and highlight basin deposits that are up to 45 ms thick (Table 2 and Fig. 6). The latter seismic facies is associated with clinothems developed in the late phase of the PRLW progradation (Fig. 6).

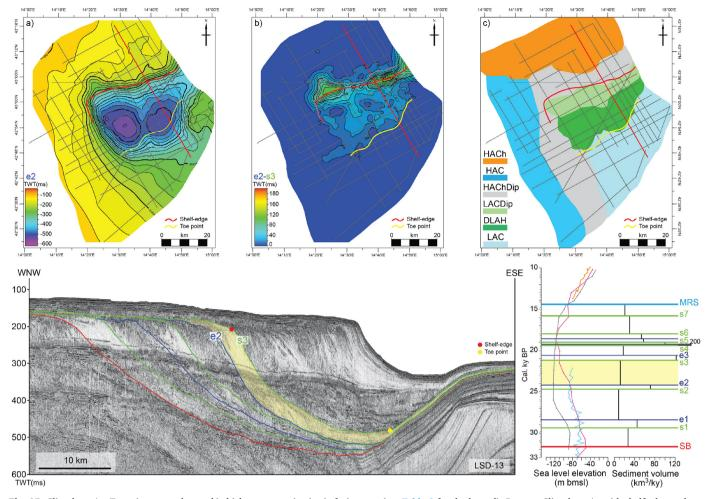


Fig. 15. Clinothem  $A_3$ . Top: a) structural map; b) thickness map; c) seismic facies map (see Table 2 for the legend). Bottom: Clinothem  $A_3$  with shelf-edge and toe points (red and yellow dot, respectively). The time spanned by Clinothem  $A_3$  along with sediment volume (km $^3$ /ky) and eustatic curves are highlighted in yellow. For references of eustatic curves see Fig. 11 caption. (For interpretation of the references to color in this figure legend, the reader is referred to the Web version of this article.)

#### 4.3.6. Lower foreset-bottomset inferred depositional environment

The SHAM, DLAH, and HLAC seismic facies are interpreted as slope-deep-marine facies. In particular, SHAM and DLAH are interpreted as Distributary channel-Lobe Complexes (DLCs), and as Mass Transport Complexes (MTCs), respectively, based on their close resemblance to core-calibrated seismic facies found in basin-floor fan deposits in the Gulf of Mexico (Prather et al., 1998; Beaubouef and Friedmann, 2000). HLAC seismic facies suggest the presence of concordant heterolithic strata in the younger clinothems (Fig. 6).

#### 4.3.7. Bottomset seismic facies (HLAC)

At the basinward end of clinothems High- and Low-Amplitude Continuous reflections (HAC and LAC) characterize the sedimentary packages (Fig. 6).

#### 4.3.8. Bottomset inferred depositional environment

This facies has been calibrated by extensive coring as muddy basinal facies with black fine-grained intercalations (Trincardi et al., 1996; Piva

et al., 2008a, b). Fairly continuous (but variable rate) sedimentation promoted continuous bottomset aggradation in the easternmost portion of the PRLW (Gallignani-Pelagosa sector; Fig. 4).

#### 4.4. Evolution of the PRLW

## 4.4.1. The mid Adriatic deep 31.8 cal. ky BP (SB surface) and the PRLW total thickness

At 31.8 ky BP, the MAD was a semi-elliptical slope basin about 45 km long and 40 km wide with a maximum paleo-depth of ca. 450 m (Pellegrini et al., 2017b, Fig. 10). The gently dipping shelf passed into a slope dipping about 1°, and to a pronounced bowl-shaped topography in the central sector of the basin, which hosted a central NNE-SSW anticline structure that we term the "MAD anticline" (Fig. 10). The PRLW accumulated in the MAD reaching 350 m in thickness ( $> 400 \, \mathrm{ms}$ ; Fig. 10) for a total accumulation of  $504 \, \mathrm{km}^3$ .

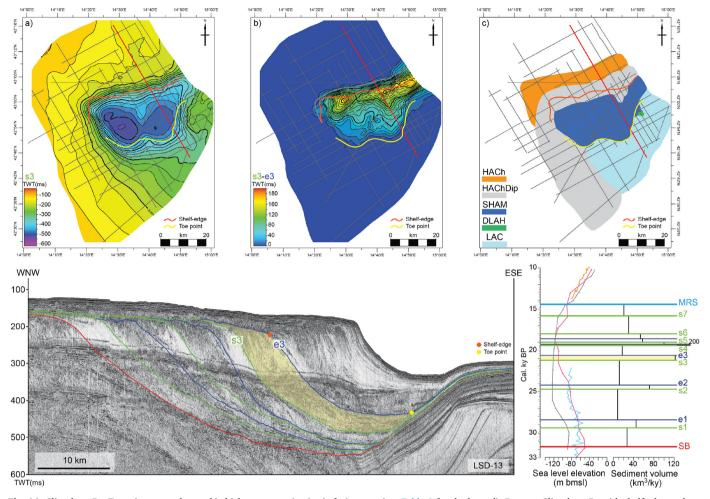


Fig. 16. Clinothem  $B_3$ . Top: a) structural map; b) thickness map; c) seismic facies map (see Table 2 for the legend). Bottom: Clinothem  $B_3$  with shelf-edge and toe points (orange and yellow dot, respectively). The time spanned by Clinothem  $B_3$  along with sediment volume (km $^3$ /ky) and eustatic curves are highlighted in yellow. For references of eustatic curves see Fig. 11 caption. (For interpretation of the references to color in this figure legend, the reader is referred to the Web version of this article.)

#### 4.4.2. Clinothem characterization

Within the PRLW we recognize three types of elemental shelf-edge clinothems based on their topset geometry, shelf-edge and onlap-point trajectory and seismic facies. The following paragraphs describe the three types of elemental shelf-edge clinothems, highlighting map pattern of sediment distribution, and lateral extent of seismic facies and inferred depositional environments for each of the thirteen elemental clinothem (Figs. 11–23). For a detailed description of each elemental clinothem the reader is referred to Table 3 and Table 4a, b, and to the supplemental material. The elemental clinothems are separated by key regional surfaces categorized as "e" and "s" surfaces based on the change in shelf-edge trajectory across them. The character, significance, and timing of the surfaces are described in detail in Pellegrini et al. (2017a).

Type A clinothems are characterized by foreset inclination between 0.9° and 2.1° and show an ascending shelf-edge trajectory coupled with a landward shift of coastal onlap (see thickness maps of type A clinothems in Figs. 11, 13, 15, 17, 19 and 21). The thickness maps of type A clinothems show topset aggradation, typically 10 m at the shelf-edge,

over an average distance of 10 km and range in plan view from radial (e.g. clinothem  $A_1$ ; Fig. 11), to E-W elongated and digitate (e.g. clinothem  $A_3$ ; Fig. 15), to elliptical (e.g. clinothem  $A_6$ ; Fig. 21). The depocenter reaches a maximum of 160 ms (ca. 120 m) in  $A_2$  clinothem, and is located in a different sector of the slope (Figs. 11, 13, 15, 17, 19 and 21)

The seismic facies maps of type A clinothems show the presence of the HACh topset facies (orange sectors in the seismic facies maps, denoting amalgamated channels on a broad coastal plain) located landward of the shelf-edge both NW and WSW of the MAD, along with isolated incised valleys containing internal oblique reflections (Fig. 9). As an exception, clinothems  $A_3$ ,  $A_5$  and  $A_6$  show HAC reflections recording delta plain deposits (blue sectors in Figs. 15c, 19c and 21c). The foreset is predominantly characterized by HAChDip corresponding to a channelized slope (grey sectors in Figs. 11c, 13c and 15c, 17c, 19c, and 21c). The bottomsets of type A clinothems are characterized chiefly by DLAH reflections indicating the presence of Mass Transport Complexes (MTCs). The MTCs appear either: i) confined east of the central-MAD antiform and lapping onto the southern margin of the basin (clinothems

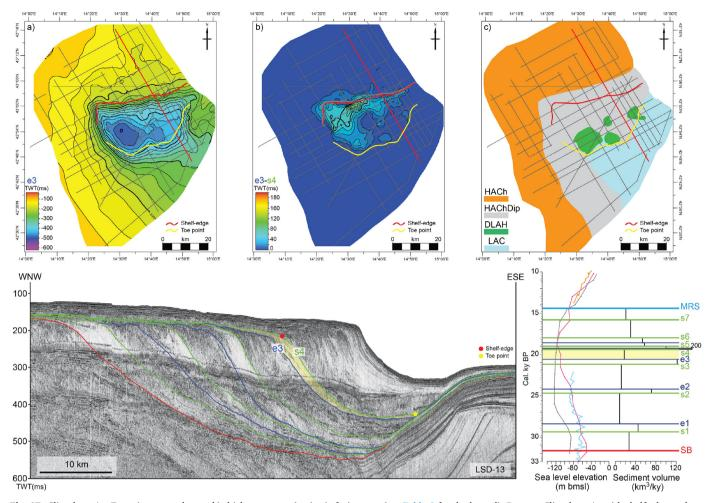


Fig. 17. Clinothem  $A_4$ . Top: a) structural map; b) thickness map; c) seismic facies map (see Table 2 for the legend). Bottom: Clinothem  $A_4$  with shelf-edge and toe points (red and yellow dot, respectively). The time spanned by Clinothem  $A_4$  along with sediment volume (km $^3$ /ky) and eustatic curves are highlighted in yellow. For references of eustatic curves see Fig. 11 caption. (For interpretation of the references to color in this figure legend, the reader is referred to the Web version of this article.)

 $A_1$ ,  $A_2$ , and  $A_6$ ; green sector in Figs. 11c, 13c and 21c, respectively); or ii) extended over large bottomset sectors (clinothems  $A_3$  and  $A_5$ ; Figs. 15 and 19); or iii) with an erratic distribution (clinothem  $A_4$ ; Fig. 17). The distal seismic facies is characterized by HAC and LAC reflections that are the evidence fine-grained deposition (blue and light-blue sectors, respectively, in Figs. 11c, 13c and 15c, 17c, 19c, and 21c).

Type B clinothems are characterized by foreset inclinations between  $1^\circ$  and  $2^\circ$  and have a flat to descending shelf-edge trajectory coupled with a maximum distance of < 5 km between the shelf-edge and correlative onlap point (where the "e" surface merges with the underlying "s" surface; Figs. 12, 14, 16, 18 and 20). The thickness maps of type B clinothems do not display topset aggradation and vary from radial (e.g. clinothem  $B_1$ ; Fig. 12) to E-W elongated and digitate external spatial distribution (e.g. clinothem  $B_4$ ; Fig. 18). The depocenter reaches a maximum value of 220 ms (ca. 160 m) in clinothem  $B_1$ , and are located mainly in the upper slope (Figs. 12, 14, 16, 18 and 20).

The seismic facies maps of type B clinothems show the presence of a restricted area NW of the MAD characterized by seismic facies with HACh reflections (orange sectors correspond to amalgamated channels

on a restricted coastal plain). The foreset that show HAChDip reflections are interpreted as slope channels (grey sectors in Figs. 12c, 14c and 16c, 18c, and 20c) that pass basinward to SHAM reflections ascribed to Distributary Channel-Lobe Complexes (DLCs, dark blue sectors in Figs. 12c, 14c and 16c, 18c, and 20c). In the eastern sub-basin DLCs dominate and extend to the southern limit of the slope basin where they pass to HAC and LAC reflections, most like fine-grained deposits, toward the southern margin of the MAD basin (blue and light-blue sectors, respectively, in Figs. 12c, 14c and 16c, 18c, and 20c).

Type C clinothems are characterized by foreset inclinations between  $1.9^{\circ}$  and  $2^{\circ}$  and show sharply ascending shelf-edge trajectory coupled with a landward shift of coastal onlap (see thickness maps of type C clinothems in Figs. 22 and 23). The thickness maps of type C clinothems show an average topset aggradation of 15 m over a distance of > 20 km, and range from E-W elongated to elliptical external geometry (clinothems  $C_1$  and  $C_2$  in Figs. 22 and 23, respectively). The depocenter reaches a maximum value of 200 ms (ca. 150 m) in  $C_1$  clinothem, and are located in the upper slope (Figs. 22 and 23).

The seismic facies maps of type C clinothems shows the presence of

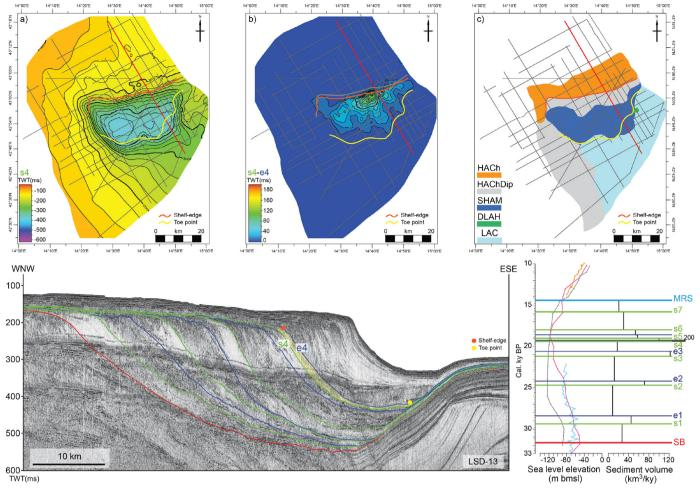


Fig. 18. Clinothem  $B_4$ . Top: a) structural map; b) thickness map; c) seismic facies map (see Table 2 for the legend). Bottom: Clinothem  $B_4$  with shelf-edge and toe points (orange and yellow dot, respectively). The time spanned by Clinothem  $B_4$  along with sediment volume (km $^3$ /ky) and eustatic curves are highlighted in yellow. For references of eustatic curves see Fig. 11 caption. (For interpretation of the references to color in this figure legend, the reader is referred to the Web version of this article.)

HACh reflections that pass to HAC reflections suggesting the confinement of amalgamated channels in the western topset in  $C_1$  clinothem (Fig. 22c); and HAC and HAD reflections in the topset of  $C_2$  clinothem representing deltaic and coastal, and lagoonal deposits, respectively. The deltaic and coastal deposits are characterized of fine-medium and clean sand (see detail of sediment core in Fig. 24). On the foreset, type C clinothems show a variety of seismic facies from LACDip to HACWDip reflections reminiscent of muddy to sandy slope deposits that locally are characterized by crenulation features (sensu Urgeles et al., 2011, Figs. 22 and 23). The distal seismic facies in the toe of the foreset are characterized by LAC reflections of fine-grained deposits (Figs. 22 and 23).

The three types of elemental clinothems are systematically stacked in an accretionary pattern with type A and B clinothems, that constitute Clinothem Set 1 (31.8–18.0 cal. ky BP), characterized by a flat/slightly falling shelf-edge trajectory and a shelf-edge progradation of ca. 30 km; type C clinothems, composing Clinothem Set 2 (18.0–14.4 cal. ky BP), shows instead an ascending shelf-edge trajectory and a maximum shelf-edge progradation of ca. 10 km (Fig. 6). Altogether, through the

deposition of Clinothem Sets 1 and 2 the shelf-edge prograded seaward a total of  $40\,\mathrm{km}$  in ca. 17,000 years.

#### 4.4.3. The Mid Adriatic Deep: modern configuration

The modern bathymetry is characterized by a straight 35-km shelf-edge in the north, a western slope sector characterized by the presence of crenulated features, and a narrow 254-m deep slope-basin bounded to the east and to the south by the complex Gallignani-Pelagosa relief of tectonic origin. The multibeam data (Fig. 10) document a widespread field of pockmarks (Fig. 24), confirming the escape of fluids through the underlying units (Hovland and Curzi, 1989; Trincardi et al., 2004; Geletti et al., 2008).

A comparison of the modern bathymetry with the paleobathymetry of the MAD at 31.8 ky BP, reveals that macro changes of the basin configuration occurred mainly through the progressive southward shift of the northern rim of the basin, reflecting 40 km progradation of the shelf-edge (Fig. 24). Conversely, the configuration of the southern boundary of the basin remained substantially fixed, reflecting an area of fine-grained sediment aggradation. As a consequence, the basin size

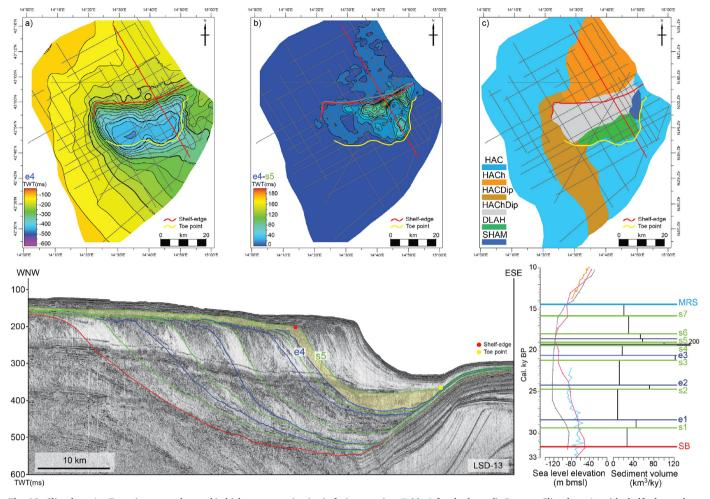


Fig. 19. Clinothem  $A_5$ . Top: a) structural map; b) thickness map; c) seismic facies map (see Table 2 for the legend). Bottom: Clinothem  $A_5$  with shelf-edge and toe points (red and yellow dot, respectively). The time spanned by Clinothem  $A_5$  along with sediment volume (km $^3$ /ky) and eustatic curves are highlighted in yellow. For references of eustatic curves see Fig. 11 caption. (For interpretation of the references to color in this figure legend, the reader is referred to the Web version of this article.)

shrunk from ca. 3500 to  $1600\,\mathrm{km}^2$  (this measure is taken comparing the areas surrounded by the  $200\,\mathrm{m}$  bathymetric contour at  $31.8\,\mathrm{ky}$  BP and today).

#### 5. Discussion

#### 5.1. History of the PRLW: patterns, influences, and controls

The development of the PRLW occurred in four main phases recorded by integrated changes in stratal-stacking patterns, shelf-edge trajectory, map-pattern distribution of sediment accumulation, character of the strata within the clinothems, and basin environmental conditions. These phases appear to be closely related to changes in both accommodation and sediment supply, as conditioned by pre-existing bathymetry, eustasy, oceanographic conditions, and global and regional climate. Oceanographic conditions of importance to stratal character included salinity, temperature, turbidity, nutrient availability, and dominant energy mode (waves, river, or tides). Integration of the broad range of controls and influences revealed the genesis of the stratal

patterns and enables appropriate use of the PRLW as an analogue for prediction of rock properties in ancient systems. The following section discusses the main patterns, influences, and controls of each phase of development of the PRLW. Table 4a and b presents details of each clinothem and associated paleoenvironment regime, respectively.

For completeness, we briefly describe the strata that occur below the basal Sequence Boundary (SB): The stratigraphic unit below SB has been interpreted as a regressive succession of subaqueous muddy clinothems that accumulated on the shelf under the influence of alongshore sediment transport during the last phase of the Pleistocene eustatic fall (Trincardi and Correggiari, 2000; Ridente et al., 2009). These subaqueous muddy clinothems were genetically related to subaerial progradation nourished by the ancestral Po River (Pellegrini et al., 2017b). This interpretation is supported by the overall external geometry of this unit, its seismic facies, and the location of the shoreline during its deposition (> 15 km from the shelf-edge; Pellegrini et al., 2017b). The microfaunal assemblages recorded in the PRAD1-2 borehole below SB confirm an outer shelf paleoenvironment with bottom waters relatively well oxygenated and warm surface waters

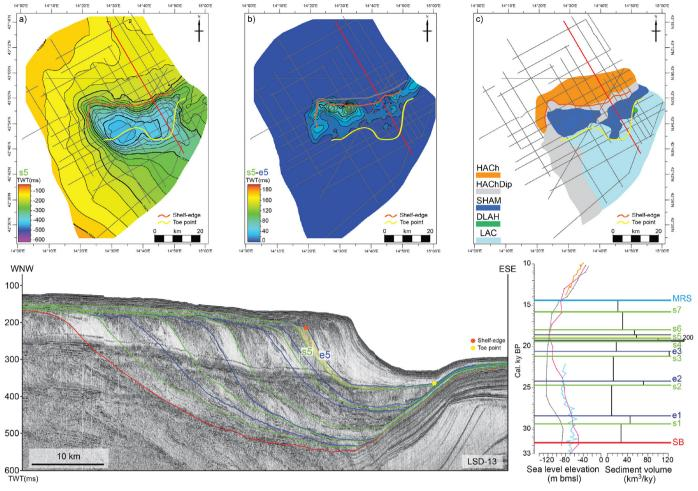


Fig. 20. Clinothem  $B_5$ . Top: a) structural map; b) thickness map; c) seismic facies map (see Table 2 for the legend). Bottom: Clinothem  $B_5$  with shelf-edge and toe points (orange and yellow dot, respectively). The time spanned by Clinothem  $B_5$  along with sediment volume (km $^3$ /ky) and eustatic curves are highlighted in yellow. For references of eustatic curves see Fig. 11 caption. (For interpretation of the references to color in this figure legend, the reader is referred to the Web version of this article.)

characterized by winter mixing during the early phase of MIS 3 (59-40 ky BP; Piva et al., 2008b). This condition evolves after 40 ky BP into a shallower (mid-shelf) environment with progressively colder, more productive and stratified surface waters (Piva et al., 2008b).

## 5.1.1. Phase 1: basal Sequence Boundary (SB) to s2 (clinothems $A_1$ to $A_2$ ), 31.8 to 24.7 ky BP

**Patterns:** The strata between surfaces SB and s2 comprise two type A and one type B clinothems that stack in an overall progradational pattern. The shelf-edge trajectory evolves from flat to slightly ascending to slightly descending. In plan view, sediment accumulation evolves from a radial pattern restricted to the central outer shelf with compensational stacking of clinothems  $A_1$  and  $B_1$ , to linear progradation in the eastern slope area in  $A_2$  clinothem (Figs. 11–13; Table 4a). The upstream (topset) region is interpreted to have been a broad coastal plain with amalgamated channel belts of the Po River (more preserved from the NW) and the Apennine rivers (less preserved from the WSW) converging to the Mid-Adriatic Dip (MAD). The foreset region was a channelized sandy slope environment. The proximal bottomset region

includes stacks of Mass-Transport Complexes (MTCs in  $A_1$  and  $A_2$ ) and Distributary Channel-Lobe Complexes (DLCs in  $B_1$ ), whereas the distal bottomset area accumulated conformable fine-grained strata.

Influences and controls: At the onset of the deposition of Phase 1 the basin morphology was influenced by the presence of the MAD antiform that extended SSE from the shelf-edge to the base of the slope. This antiform separated the MAD into two sub-basins that are prominent at the base of the interval, but progressively more subdued upward. Eustasy fell by 45 m-125 m below present-day sea level quite rapidly at the beginning of this phase (A1), and continued to fall, but more slowly during the upper two-thirds of this phase (A2; Lambeck et al., 2014). This fall corresponds globally to the end of Dansgaard-Oeschger Interstadial 5 (based on lighter  $\delta^{18}$ O values and an abundance peak of warm planktic species at this level in the PRAD1-2 borehole), followed by a phase of rapid and continued growth of the Laurentide and European ice sheets (Dyke et al., 2002; Boulton et al., 2001). Sediment supply rates to the basin increased significantly at the base of the interval, and decreased towards the top by a factor of 5; sediment accumulation rates vary from 27.5 to 44 to 9 km<sup>3</sup>/ky upward in the

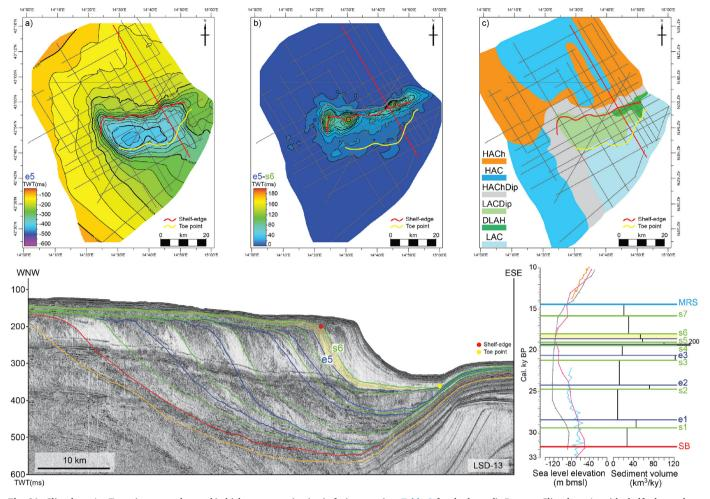


Fig. 21. Clinothem  $A_6$ . Top: a) structural map; b) thickness map; c) seismic facies map (see Table 2 for the legend). Bottom: Clinothem  $A_6$  with shelf-edge and toe points (red and yellow dot, respectively). The time spanned by Clinothem  $A_6$ along with sediment volume (km $^3$ /ky) and eustatic curves are highlighted in yellow. For references of eustatic curves see Fig. 11 caption. (For interpretation of the references to color in this figure legend, the reader is referred to the Web version of this article.)

three  $A_1$ ,  $B_1$ , and  $A_2$  clinothems, respectively (Table 4b). Regionally, the Apennine glaciers were advancing throughout Phase 1, with Alpine glaciers starting their advance slightly later, during  $A_2$  time (Fig. 8; Table 4b; Giraudi, 2017; Monegato et al., 2017).

The planktic assemblage, not abundant, indicates that surface waters were cold and biogenically productive (Hemleben et al., 1989; Pujol and Vergnaud-Grazzini, 1995), at least far from direct riverine influence, as suggested by the dominance of the opportunistic benthic foraminifera species *C. carinata* (Fig. 8; Table 4b; Van der Zwaan and Jorissen, 1991, Mojthaid et al., 2009, Goineau et al., 2011). Bottom waters appear to have been relatively well oxygenated, with organic matter being decreasingly well preserved upward (Fig. 8). This interpretation is based on the peaks of the epifaunal/shallow infaunal foraminifer *H. balthica* that suggest relatively well-oxygenated bottom water and/or a lowering of the quality of the organic matter (Schmiedl et al., 2000; Hess and Jorissen, 2009; Murray, 2006; Sweetman et al., 2009). Starting abruptly from 28.2 ky BP (corresponding ca. to the e1 surface, Fig. 8) conditions became less favorable, in particular for the intermediate-water dweller *G. bulloides* (much less abundant from this

level upward) driven by a progressive decrease of the water depth (Fig. 8; i.e. the low and steady SAR in PRAD1-2 rules out a dilution of the planktic foraminifera). This shift matches the beginning of the Global LGM, coeval with Greenland Stadial 3 (27.540–23.340 ka) and encompasses the global sea-level lowstand (Hughes and Gibbard, 2015).

#### 5.1.2. Phase 2: s2-s5 (clinothems $B_2$ to $A_5$ ), 24.7 to 19.0 ky BP

**Patterns:** The strata between surfaces s2 and s5 comprise three type A as well as three type B clinothems that stack in an overall progradational pattern. The shelf-edge trajectory alternated between descending in type B clinothems to slightly ascending in type A clinothems. In plan view, sediment accumulation evolved from three main radial depocenters on the slope of  $B_2$  clinothem to elliptical depocenters slightly elongated W-E and with a digitate map pattern. For the first time since the PRLW progradation began, clinothems depocenter started to reflect a structural confinement against the distal limit of the basin (southern rim). In addition,  $A_4$ - $B_4$ - $A_5$  clinothems are reduced in thickness and extent compared to the previous couplets, and show clear

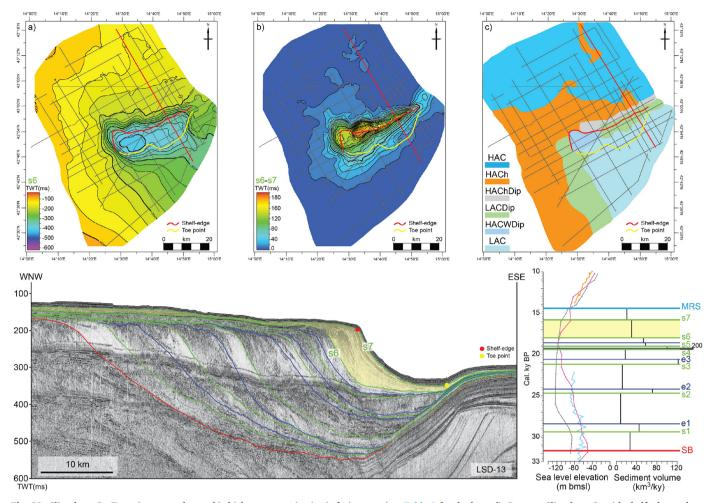


Fig. 22. Clinothem  $C_1$ . Top: a) structural map; b) thickness map; c) seismic facies map (see Table 2 for the legend). Bottom: Clinothem  $C_1$  with shelf-edge and toe points (red and yellow dot, respectively). The time spanned by Clinothem  $C_1$ along with sediment volume (km<sup>3</sup>/ky) and eustatic curves are highlighted in yellow. For references of eustatic curves see Fig. 11 caption. (For interpretation of the references to color in this figure legend, the reader is referred to the Web version of this article.)

compensational patterns (Figs. 17-19; Table 4a). The topset region is interpreted to have been a broad coastal plain with amalgamated channel belts of the Po River (to the NW) and the Apennine rivers with occasionally-preserved delta plain sandy-silt deposits converging to the MAD. Upward in the topset sector, clinothems evolved from those dominated by amalgamated channel-belt deposits (A3 clinothem; Fig. 25), to isolated incised valleys with internal point-bar migration that suggest a switch of the fluvial systems to more sinuous, meandering patterns (A5 clinothem; Fig. 25). In the foreset area, large-scale turbidite slope channel-levee complexes covered by mud wedges (B2 clinothem; Fig. 25) record the closest linkage of the shelf to the basin during PRLW progradation. proximal the entire The bottomset alternated between Mass-Transport Complexes (MTCs in A<sub>3</sub>, A<sub>4</sub>, and A<sub>5</sub>) and Distributary Channel-Lobe Complexes (DLCs in B<sub>2</sub>, B<sub>3</sub>, and B<sub>4</sub>). The distal area shows a change in seismic facies character of the conformable fine-grained strata from HAC to LAC reflections for most of this phase.

*Influences and controls:* Pre-existing bathymetry was subtly influenced by the sea-floor expression of the MAD antiform with the western sub-basin deeper than the eastern sub-basin up to the progradation of

B<sub>4</sub> clinothem after which the MAD antiform was expressed mainly in the bottomset sector (Figs. 14-19). Eustasy continued to fall slowly down to 135 m below present-day sea level (Lambeck et al., 2014) during the first half of this phase (B2-B3) until reaching stillstand during accumulation of clinothems A4 to A5 (Fig. 8). This eustatic phase reflected an interval of increasing ice volume of the Laurentide and Scandinavian ice sheets (Dyke et al., 2002; Boulton et al., 2001, respectively). Sediment composition changed at the beginning of Phase 2 (surface s2, 24.7; Fig. 8) when Ca/Ti and K/Ti ratios increased abruptly. We interpret these shifts to reflect a change of the weathering intensity and a major change of sediment provenance probably driven by the maximum advance of Alpine glaciers documented at 25 ky BP by Monegato et al. (2017). In turn, this evidence suggests a very small buffering time (i.e. delay) between catchment and sink areas. Sediment supply rates in Phase 2 changed as well, showing alternating increases and decreases that were one order of magnitude larger in type B clinothems than in type A clinothems. In particular, Clinothem B4 attained the maximum SAR of 200 km<sup>3</sup>/ky for the entire PRLW (Table 4b). Regionally, during Phase 2 Alpine and Apennine glaciers were waxing and waning (Fig. 8; Table 4b; Giraudi, 2017; Monegato et al., 2017).

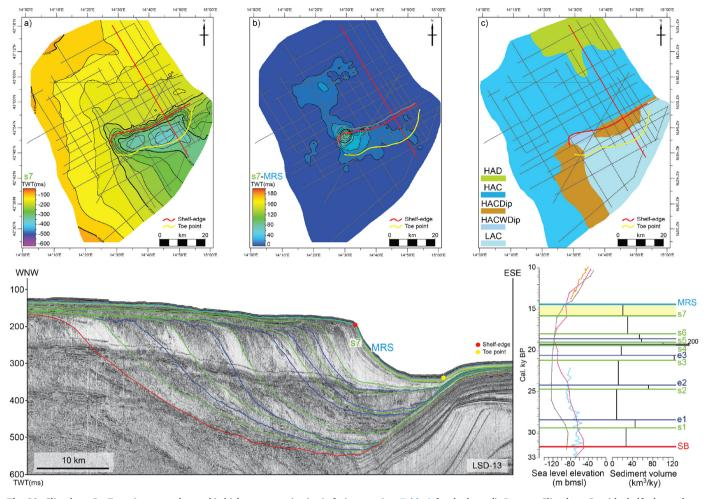


Fig. 23. Clinothem  $C_2$ . Top: a) structural map; b) thickness map; c) seismic facies map (see Table 2 for the legend). Bottom: Clinothem  $C_2$  with shelf-edge and toe points (red and yellow dot, respectively). The time spanned by Clinothem  $C_2$  along with sediment volume (km<sup>3</sup>/ky) and eustatic curves are highlighted in yellow. For references of eustatic curves see Fig. 11 caption. (For interpretation of the references to color in this figure legend, the reader is referred to the Web version of this article.)

The microfaunal assemblages indicate that surface waters were still cold and productive (Fig. 8; Table 4b). In contrast to Phase 1, however, bottom waters during Phase 2 were affected by reduced ventilation (as indicated by the concurrent abundance peaks of the deep-infaunal species; Fig. 8), reflecting the onset of millennial-scale (from B<sub>2</sub> upward) up to centennial-scale (from B<sub>4</sub> upward) fluctuations of riverine input, witnessing a marked environment variability. This interpretation is based on a decreasing concentration of planktic foraminifera coupled with the minima in abundance of *C. carinata* and concurrent peaks of *N. depressulus* and *N. pauciloculum*, indicative of inner shelf to estuaries/lagoons environments (Fig. 8; Hohenegger et al., 1989, Murray, 2006). Moreover, foraminifera *N. depressulus* and *N. pauciloculum* are more common (at intervals even abundant) and continuously distributed compared to the Phase 1, indicating that riverine discharge was closer to the borehole site.

#### 5.1.3. Phase 3: s5 to s6 (clinothems $B_5$ to $A_6$ ), 19.0 to 18.0 ky BP

**Patterns:** The strata between surfaces s5 and s6 comprise one type B and one type A clinothems stacked in an overall progradational to

aggradational pattern. The shelf-edge trajectory evolves from slightly descending to ascending. In plan view, sediment accumulation occurs mainly in elliptical, coalescing depocenters that extended to the upper slope and were restricted to the western sub-basin (Figs. 20 and 21; Table 4a). The topset region is interpreted as a local coastal plain with amalgamated channel belts of the Po River (more preserved to the NW) coupled with delta plains of the Apennine rivers (more preserved to the WSW) converging to the MAD. The foreset region appears to have evolved from sandy to muddy prodelta-slope and the proximal bottomset region shifts from Distributary Channel-Lobe Complexes (DLCs in  $\rm B_5)$  to Mass-Transport Complexes (MTCs in  $\rm A_6)$ . The distal bottomset area accumulated LAC reflections interpreted as conformable finegrained strata.

*Influences and controls:* Pre-existing bathymetry was subtly influenced by the sea-floor expression of the MAD antiform in the bottomset area with the western sub-basin still being deeper than the eastern one. Eustasy began to rise with a jump of 15 m at the onset of Clinothem  $B_5$  (19 ky BP). The beginning of eustatic rise corresponds globally to the first melt-water pulse (MWP-1), ascribed to the partial collapse of the

Table 3
Summary of the characteristics of the elemental of

Clinothen	Clinothem Interval span (cal.ky)	Maximum Thickness (m)	Volume (km³) Maximum (km³/yr)	Maximum Accummulation Rates $(km^3/yr)$	Average shelf-edge progradation (km)	Foreset inclinatioin (°) Depocenter	Depocenter
ర	1.4	64	30	21.5	1.1	2	Elliptical, restricted on the western slope
ڻ ت	2.2	150	29	30.5	5.5	1.9	E-W elongated, convey the structural confinement in the western sub-basin
$A_6$	9.0	85	33.5	56	က	1.9	Elliptical in western sub-basin and elongated in the eastern one
$\mathbf{B}_{5}$	0.4	78	23	57.5	4	2	On the western upper slope, compensational compared to A <sub>5</sub>
$A_5$	0.3	80	30	100	0.5	1.8	Coalescent depocenters on the slope
B <sub>4</sub>	0.1	82	20	200	1.5	1.8	Elongated on the central slope, digitate external geometry, compensational compared to $A_4$
A <sub>4</sub>	1.2	75	21	17.5	1.5	1.6	On the western slope, reflecting the structural confinement at the toe
$\mathbf{B}_3$	0.5	136	61	122	6.5	1.8	Coalescing depocenters E-W elongated and with digitate external geometry
$A_3$	3.1	06	40	13	3	2.1	Two main depocenters on the slope, digitate external geometry
$\mathbf{B}_2$	0.5	95	36	72	4.5	1.8	Three main depocenters on the slope
$A_2$	3.7	120	33	6	2.6	1.5	Restricted on the eastern slope
$\mathbf{B}_{1}$	1.0	160	44	44	3.2	1	Radial, compensational compared to A <sub>1</sub>
$A_1$	2.4	110	99	27.5	3.8	6.0	Radial, restricted on the central outher shelf

Northern Hemisphere ice sheets (Yokoyama et al., 2000; Tarasov and Peltier, 2004; Bard et al., 1996; Carlson and Clark, 2012), followed by a phase of eustatic rise with rates of ca.  $12\,\mathrm{m/ky}$  (Lea et al., 2002; Mitrovica, 2003; Siddall et al., 2003; Peltier and Fairbanks, 2006; Bard et al., 2010; Lambeck et al., 2014; Benjamin et al., 2017). Sediment-supply rates to the basin remained substantially constant with sediment-accumulation rates of 57.5 and  $56\,\mathrm{km^3/ky}$  in  $B_5$  and  $A_6$ , respectively (Table 4b). Regionally, glaciers were retreating in the Alps and the extent of Apennine glaciers was approaching zero (Fig. 8; Table 4b; Giraudi, 2017).

The microfaunal assemblage indicates that surface waters continued to be cold and productive (Fig. 8; Table 4). Bottom waters were still affected by minor ventilation (as indicated by the concurrent abundance peaks of the deep-infaunal species; Fig. 8). Fresh-water supply condition were similar to the preceding Phase 2, whereas the abrupt drop in abundance of *C. carinata* suggests variations in water environmental parameters such as salinity and turbidity.

#### 5.1.4. Phase 4: s6 to MRS (clinothems $C_1$ to $C_2$ ), 18.0 to 14.4 ky BP

Patterns: The strata between surfaces s6 and MRS comprise two type C clinothems stacked in an overall aggradational pattern. The shelf-edge trajectory is markedly ascending. In plan view, sediment accumulation evolves from an E-W elongated depocenter to a more elliptical depocenter on the slope, coupled with aggradation of the topsets of both clinothems on a broad area of the northwestern shelf (Figs. 22 and 23; Table 4a). During the progradation of type C clinothems their topsets aggraded up to 45 m —the thickest and most extensive aggradation of the entire PRLW. The topset is interpreted as sandy deltaic and coastal deposits where the Po and Apennine channels tended to become isolated, narrower, and thinner with more subdued levees than those in the underlying clinothems (Fig. 25). The foreset region comprises heterolithic prodelta-slope deposits characterized by crenulation features possibly reflecting density flows (Fig. 24, and Mulder and Syvitski, 1995). The proximal bottomset region evolved to strata that are conformable with the underlying clinothems (where DLCs in B clinothems and MTCs in A clinothems are preserved). The distal bottomset area is characterized by LAC reflections interpreted as conformable fine-grained strata, similar to preceding Phase-3 strata.

Influences and controls: During this phase, the pre-existing bathymetry evolved to a surface where the MAD antiform was almost buried. Eustasy continued to rise with rates of up to 12 m/ky (e.g. Lambeck et al., 2014) followed by an event of accelerated eustatic rise at ca. 14.5 ky BP to a rate of several m per century (Clark et al., 2004). This accelerated rise has been attributed to meltwater pulse (MWP-1A; Fairbanks, 1989; Lambeck et al., 2014) after the onset of the Bølling-Allerød warm period; it coincided with the formation of the MRS atop Clinothem C<sub>2</sub> (Fig. 8; Table 4b). Sediment-supply rates to the basin decreased towards the top of this interval by a factor of 5 relative to the preceding Phase-3 SAR; sediment-accumulation rates vary from 30.5 to a minimum of 21.5 km<sup>3</sup>/ky upward in the two C<sub>2</sub> clinothems (Table 4b), and to about zero at the MRS. Still, sediment supply played a major control in maintaining the progressive seaward shift of the shelf-edge in the early phase of post-LGM eustatic rise. In the catchment, during this interval, glaciers were rapidly retreating: the Alpine glaciers shrinking within their catchment outlets (Monegato et al., 2017) and the Apennine glaciers being already close to zero (Giraudi, 2017, Fig. 8; Table 4b).

The microfaunal assemblage indicates that surface waters was still influenced by high riverine influence. Increased fresh-water discharge during Phase 4 was probably also the main factor affecting the planktic foraminifera, which responded with 1) a markedly oligotypic assemblage dominated by the small subarctic surface dweller *T. quinqueloba* (ca. 90% on average), and 2) the absolute minima in concentration for the entire PRLW (Fig. 8; Table 4b). Bottom waters were affected by low ventilation (as indicated by the concurrent abundance peaks of the deep infaunal species; Fig. 8), reflecting centennial oscillations of riverine

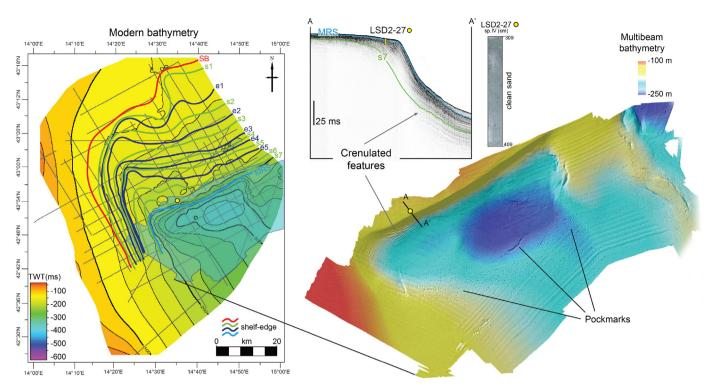


Fig. 24. The modern MAD bathymetry from seismic horizon interpolation with clinothem shelf-edge positions and types during the PRLW progradation. Progradation produced a 40 km southward shift of the shelf-edge along with the burial of MAD antiform. Detail of the modern multibeam bathymetry shows slope-parallel bedforms (crenulated features) and a widespread field of seabed pockmarks.

input. The centennial-scale oscillations in fresh-water input to the basin increased in magnitude that culminated between 18 and 16 ky BP. This trend is recorded by rapid shifts in the abundance of *Nonion* spp (Fig. 8), and very large oscillations of the  $\delta^{18}$ O composition of planktic foraminifera (up to 2 per mil towards lighter values) that reflect salinity drops during phases of enhanced fresh-water discharge. Increased freshwater input in Phase 4 is also indicated, in the shallowest coring sites, by a frequency peak of the benthic species *Ammonia perlucida* (Fig. 8) a taxon with a modern distribution restricted to very shallow shelf areas in the Adriatic Sea (< 20 m, Jorissen, 1987, 1988) and neighboring lagoon environments (Donnici et al., 1997). At ca. 14.6 ky BP an abrupt increase of the abundance and a substantial turnover of the assemblages of planktic and benthic foraminifera in all three coring sites records the drowning and abandonment of the PRLW (MRS at 14.4 ky BP; Fig. 8; Table 4a, b).

The abandonment of the PRLW coincides with a period of high-rate eustatic rise dated at ca. 14.5 ky BP (Lambeck et al., 2014) just before the Bølling-Allerød warm period (Table 4a, b). This was followed by the formation of barrier lagoon systems (Storms et al., 2008) and by the progradation of compound deltas on the mid-shelf (Pellegrini et al., 2015).

## 5.2. Variations of the distance between shoreline and its time-equivalent shelf-edge

Earlier publications dealing with delta systems have tried to predict the nature of basinal deposits by analyzing specific indicators such as coastal-onlap and shelf-edge trajectory, and foreset dip (e.g. Helland Hansen and Martinsen, 1996; Plink-Björklund et al., 2001; Porebski and Steel, 2003; Johannessen and Steel, 2005; Carvajal and Steel, 2006; Ryan et al., 2009; Patruno et al., 2015; Poyatos-Moré et al., 2016; Gong et al., 2016 for a review; Anell and Midtkandal, 2017). Stratigraphic analyses commonly interpret stratal architecture and sediment distribution as results of the interaction of accommodation and sediment supply, but typically assume sediment-supply rates as constant. Sediment supply to a basin can, however, vary over time in response to autogenic and allogenic processes (e.g Muto and Steel, 1997; Jerolmack and Paola, 2010; Calves et al., 2013). Additionally, the supply to a basin may be out of phase with eustatic changes promoting geometrical variations at local scale (Madof et al., 2016). The PRLW represents an ideal site for deciphering detailed relations among topset geometry, shelf-edge trajectory, and basinal deposits, and to extract scaling factors related to the different type of clinothems (Pellegrini et al., 2017a). During much of PRLW progradation, the shoreline was located near the shelf-edge and a significant amount of sediment was delivered to the basin floor (Pellegrini et al., 2017b). Our work suggests that even when the shoreline was in that area, small, subtle changes in the distance between shoreline and the shelf-edge resulted in distinctive topset geometries associated with specific types of basinal deposits (Fig. 26). We conclude that when the shoreline was between 5 and 10 km from the shelf-edge, margin destabilization and formation of MTCs were likely promoted (Fig. 26; type A clinothem). During times with physiographic settings where the shoreline was closer than 5 km to the shelf-edge, topset degradation coupled with high sediment bypass to the basin promoted the formation of DLCs (Fig. 26 type B clinothems). Finally, when the shoreline was more than 10 km from the shelf-edge,

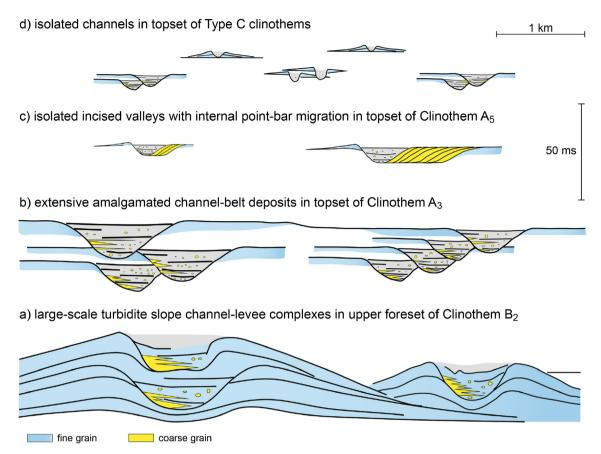


Fig. 25. Schematic diagram with feeder systems idealized from seismic lines. Note the decrease in size of feeders from bottom to the top of the succession and the deepening upward trend showing large-scale turbidite channel-levee complexes on the foreset (Clinothem  $B_2$ ); extensive acoustically transparent to chaotic units reminiscent of amalgamated channel-belt deposits up to 15 m thick (Clinothem  $A_3$ ); isolated incised valleys with a fill geometry characterized by oblique reflectors that denote point-bar migration (Clinothem  $A_5$ ); minor isolated channels, locally accompanied by subdued levees (Clinothem  $C_2$ ). During the progradation of the PRLW the main linkage between shelf and basin is preserved within  $C_2$ 0 in the most extensive fluvial unit is preserved in the topset of Clinothem  $C_3$ 1 deposited at the maximum eustatic lowstand of the last glacial.

and no direct conduit linked the shelf to the slope, no significant volume of coarse sediment reached the basin floor (Fig. 26). These values are in agreement with the independently constrained values of connection between shoreline and canyon head documented by Sweet and Blum (2016). Our finding suggests that subtle and systematic changes in the distance between shoreline and the time-correlative shelf-edge result in systematically stacked basinal deposits that in turn constitute a composite Lowstand Systems Tract that developed in only 17,000 years (Fig. 26). In this view, we show the importance of carefully analyzing both the topset geometry and the shelf-edge trajectory. (Interestingly, in the case of PRLW, the different types of clinothem are not associated with changes in the dip of the slope as documented elsewhere, e.g. Anell and Midtkandal, 2017; Ramon-Duenas et al., 2018). Our work demonstrates the potential of Quaternary successions as high-resolution frameworks from which to extrapolate scaling-factor parameters that enhance the predictability of sand-prone deposits in the basin. Whereas previous studies have focused on 100,000 year-scale cycles of glaciation-deglaciation as the temporal scale that determines the balance between shelf aggradation and sediment export to the deep basin, data from the PRLW show that sediment export to the basin can be episodic, even over centennial to millennial time-scales (Fig. 26). In this view,

our documentation demonstrates, for the first time, the minimum time interval (centennial) in which DLCs can develop with volumes on the order of 60 km<sup>3</sup> bypassing the shelf-edge (Table 3).

## 5.3. The record of composite cyclicity in the PRLW -sequence stratigraphic interpretation-

The PRLW represents a succession constrained by robust physical, bio- and chrono-stratigraphic data of high resolution (Pellegrini et al., 2017a). It thus represents an excellent natural laboratory wherein to apply the classic sequence-stratigraphic approach to decipher the complex strata of an expanded stratigraphic succession and relate them to composite cyclicity of forcing mechanisms (Fig. 27). We therefore discuss how the strata of the PRLW would be interpreted on the basis of sequence stratigraphy alone, in the absence of such detailed chronological and paleontological data, to assess how transportable are the lessons from the PRLW and what is essential to predicting the character of basin deposits based on shelfal observations. This approach follows the fundamental focus of classic sequence stratigraphy (sensu Vail et al., 1977) on the recognition of various types of stratal surfaces as foundational to stratigraphic interpretation, correlation, and mapping.

 Table 4a

 Summary of characteristics of elemental clinothems and shelf-edge trajectories within the PRLW.

Clinothem	Clinothem Pre-existing bathymetry	Depositional Patterns	Topset character; Interpretation	Foreset character, Interpretation	Proximal Bottomset character; Interpretation	Distal Bottomset Character; Interpretation	Shelf-Edge Trajectory
5	MAD antiform almost buried; two sub-basins with similar depth	Circular depocenter is in the western sub-basin and a widespread area of topset aggradation on the north-western shalf.	HAC seismic facies; sub-aqueous shelf. HAD seismic facies confined to the East; Pardic deposits	HACDip seismic facies; muddy prodelta. HACWDip seismic facies; heterolithic prodelta deposits locally characterized by crenulation features	LAC seismic facies; fine- grained basin-floor setting	LAC seismic facies; fine-grained basin- floor setting	Retrogradational Aggradational
౮	MAD antiform expressed mainly in bottomset region. Deeper sub-basin in the western sector	E.W elongated, distal area confined by structure on southern rim	HAC seismic facies mainly in the northern area and HACh seimic facies in the western area; Narrow (few tens of m wide) isolated channels, with local subdued levees (bayhead deltas in tehelrend Incom/settury)	LACDip to HACWDip reflections; muddy to sandy prodelta deposits locally characterized by crenulation features	LAC seismic facies; fine- grained basin-floor setting	LAC seismic facies; fine-grained basin- floor setting	Aggradational
$A_6$	MAD antiform expressed mainly in bottomset region. Prominent bulge at the shelf-edge and an indentiation is presents in the eastern subsain	Circular and elongated depocenters in the western and in the easten sub- basin, respectively	HAC seismic facies; data plain. HACh seismic facies; amalgamated channelbelts.	HACDip seismic facies; muddy prodelta	LACDip seismic facies; muddy prodelta. DLAH seismic facies in the easem sub-basin; Mass Transport Complexes (MTC).	LAC seismic facies; fine-grained basin- floor setting	Progradational
$\mathbf{B}_{\mathbf{S}}$	MAD antiform expressed mainly in bottomset region prominent buge at the shelf- edge	Two main coalescing depocenters in the western sub-basin extending to the upper slope; compensation compensational to A5		HACh seismic facies; Amalgamated channels. HAChDip seismic facies; sandy prodelta.	SHAM seismic facies; Distributary Lobe Complexes (DLC)	LAC seismic facies; fine-grained basin- floor setting	Degradational
$A_{\scriptscriptstyle{\mathrm{S}}}$	MAD antiform expressed mainly in bottomset region	Coalescent depocenters on slope, thickest in foreset- bottomset area	HAC seismic facies in western area; delta plain. HACh seismic facies; amalgamated channel- belts. Isolated incised valleys with oblique reflections (point-bars in meandering refreemes)	HACDip seismic facies in western area; heterolithic prodelta. HAChDip seismic facies in eastern area; sandy prodelta.	DLAH seismic facies; Mass Transport Complexes (MTC). SHAM in a restricted area; Distributary Lobe Complexes (DLC)	HAC seismic facies; fine-grained basin-floor setting	Progradational
B <sub>4</sub>	MAD antiform expressed mainly in bottomset region	Elongated on central slope, compensational to A4, digitate map pattem	(1)	HACh, HAChDip seismic facies; amalgamated channels on foreset; SHAM seismic facies; Distributary Lobe Complexes (DLC)	SHAM seismic facies; Distributary Lobe Complexes (DLC)	LAC seismic facies; fine-grained basin- floor setting	Degradational
A <sub>4</sub>	Western sub-basin deeper than eastern sub-basin	Confined to western slope, due to strucural confinement; linear progradation pattern; structural confinement at toe of clinothem	HACh seismic facies; amalgamated channel- belt deposits	HAChDip seismic facies, sandy prodelta	DIAH seismic facies; MTCs with scattered distribution	LAC seismic facies; fine-grained basin- floor setting	Progradational
$_3$	Western sub-basin deeper than eastern sub-basin	Coalescing depocenters elongated E-W with digitate map pattern; distal area confined by structure on southern rim		HAChDip seismic facies, sandy prodelta	SHAM seismic facies; Distributary Lobe Complexes (DLC)	LAC seismic facies; fine-grained basin- floor setting	Degradational
$A_3$	Western sub-basin deeper than eastern sub-basin	Two main depocenters, digitate map pattern; distal area confined by structure on southern rim	HACh in northern area; extensive acoustically transparent to chaotic units up to 15 m thick (amalgamated channel- belt deposits); HAC in eastern area; delta plain sandy-silty deposits	HAChDip seismic facies; sandy prodelta	LACDip seismic facies; muddy prodelta. DLAH seismic facies; Mass Transport Complexes (MTC)	LAC seismic facies; fine-grained basin- floor setting	Progradational

(continued on next page)

Table 4a (continued)	continued)						
Clinothem	Clinothem Pre-existing bathymetry	Depositional Patterns	Topset character; Interpretation	Foreset character, Interpretation	Proximal Bottomset character; Interpretation	Distal Bottomset Character; Interpretation	Shelf-Edge Trajectory
B <sub>2</sub>	MAD antiforms still subtly expressed	Elongated WSW-ENE on the slope area		HAChDip seismic facies, sandy prodelta; Locall parallel to wedge-shaped high-amplitude reflection packages pass laterally to low-amplitude reflections Large-scale turbidite slope channel-levee complexes coovered by mud wedges with no evidence of channelization	SHAM seismic facies; Distributary Lobe Complexes (DLC)	HAC seismic facies; fine grained basin-floor setting	Degradational
$A_2$	MAD antiform expressed as area of minimum depth on structural map	Linear progradation, restricted to eastern slope area	HACh seismic facies; analgamated channels on broad coastal plain	HAChDip seismic facies; sandy prodelta	DLAH seismic facies; Mass Transport Complexes (MTC)	HAC seismic facies; fine-grained basin-floor setting	Progradational
$\mathrm{B}_{1}$	MAD antiform still expressed in seafloor morphology	Radial, compensational to Ai (east of Ai depocenter)		HAChDip seismic facies; sandy prodelta	SHAM seismic facies; Distributary Lobe Complexes (DLC)	HAC seismic facies; fine-grained basin-floor setting	Degradational
$A_1$	MAD antiform strikes NNW- SSE from coeval shelf-edge, forming two sub-basins	Radial, restricted on the central outer shelf	HACh seismic facies; amalgamated channels; broad coastal plain NW (Po River) and WSW (Apennine rivers) of MAD	HAChDip seismic facies; channelized prodelta	DLAH seismic facies confined to area east of MAD antiform, lap onto southern margin of basin; Mass Transport Comileyes (MTC)	HAC seismic facies; fine-grained basin-floor setting	Progradational
APD							

Our sequence stratigraphic analysis interprets each B-A couplet to represent a complete high-frequency depositional sequence sensu Mitchum and Van Wagoner (1991), by associating each type B with its overlying type A clinothem (B<sub>1</sub>-A<sub>2</sub>, B<sub>2</sub>-A<sub>3</sub>, B<sub>3</sub>-A<sub>4</sub>, B<sub>4</sub>-A<sub>5</sub>, B<sub>5</sub>-A<sub>6</sub>; Fig. 27). Following strictly the usage of Mitchum et al. (1977), each sequence boundary is represented by the erosional surface at the base of a type A clinothem in the topset zone connected to the base of the immediately underlying type B clinothem at the point where the type B clinothem laps onto the underlying stratal unit, to the surface at the base of that type B clinothem in the slope and basinal zones onto which the DLC deposits lap on in the lower-slope zone and lap down in the basinal zone ('Correlation Method 1' of Martin et al., 2009). Each B-A couplet would represent Pogradational-Aggradational (PA) stacking (A<sub>1</sub> is missing its P component because it directly overlies the lower-order sequence boundary), wherein the upper surface of each type B clinothem records the change from progradation to aggradation ("e" surface; Fig. 27). The topset aggradation observed in type A clinothems reflects periods of decreased sediment supply to the slope (Table 3), as observed in model simulations from Burgess and Prince (2015). The two type C clinothems would represent parasequences (sensu Van Wagoner et al., 1990) bounded by flooding surfaces and their correlative deep-sea surfaces developed during the first phase of eustatic rise when sediment supply still keeps pace with the increase in accommodation (as discussed in the previous section). Overall, the interval from A<sub>1</sub> to A<sub>6</sub> (Clinothem Set 1) would be a progradational sequence set, and the interval from C<sub>1</sub> to C<sub>2</sub> would be an aggradational parasequence set. This interpretation was informed also considering the close geometric similarity of the PRLW strata to those seen in the XES02 experiment of Martin et al. (2009), which is illustrated in Fig. 27 and the strict application of the sequenceboundary criteria of Mitchum et al. (1977), and explains the basin-restricted stratal units. The sequence boundaries are marked by coastal onlap of type B clinothems below the pre-existing shelf-break (Fig. 27). This interpretation implies that the High Amplitude and Chaotic (HACh) seismic facies, at the most proximal part of type B clinothems, represents amalgamated distributary channels, or their subaqueous correlatives (sensu Olariu and Bhattacharya, 2006). These strata would still be near shore, because the development of DLCs on the basal surfaces of type B clinothems means that the shoreline was less than 5 km from the shelf-edge (as discussed in a previous section). Thus, the onlap of type B clinothems is effectively coastal onlap (Figs. 26 and 27). The erosion across the tops of type B clinothems would represent continuing extension of the fluvial system (the 'Ef' surface of Martin et al., 2009) within the PA/Lowstand Systems Tract, and the strata within type B clinothems is the basinal record of the diachroneity of that erosional surface (Martin et al., 2009). The "e" surface (correlation method 2 of Martin et al., 2009), although not a sequence boundary (sensu Mitchum et al., 1977), is still useful because it marks the change from progradation to aggradation within the high-frequency lowstand/PA systems tracts (we propose naming it the "P-A surface"). In addition, the landward shifts of depositional facies at the base of type A clinothems are consistent with their aggradational stacking (Figs. 26 and 27). On the minus side, this hypothesis implies that all high-frequency transgressive and highstand systems tracts (R and APD sets) were not developed at a seismically resolvable scale. This is potentially not a fatal flaw, because those are the stacking patterns and systems tracts that are least likely to be well developed under falling to low accommodation (e.g., Jervey, 1988; Van Wagoner et al., 1990; Martin et al., 2009).

The balance of evidence, plus versus minus, as well as the use of the original criteria for sequence-boundary identification (i.e., Mitchum et al., 1977) and the close match of the PRLW systems to both the stratal geometries and base-level curve of the XES02 experiment, sustains the above interpretation. The empirical, geometric-based stratigraphic framework thus constructed provides a powerful tool for predicting the nature and distribution of basinal deposits based on observations of shelfal strata, even in the absence of chronometric data. Ultimate confirmation of our sequence stratigraphic interpretation

 Table 4b

 Summary of global events, eustasy, sediment supply, water character and regional climate regime during the PRLW clinothems progradation.

Global Events	Eustasy	Sediment Supply	Surface-water Character	Bottom-water Character	Water Depth Changes	Regional Climate	Interval Age Span (cal. ky)	Surface Age (cal. ky)	SAR (km3/ky)
Meltwater pulse 1 A (MWP 1 A)	Fast rise	Substantial decrease: abandonment of the system	Warmer water		Abrupt Increase			v 14.4 v	
Onset of Termination IA (T-IA)	Fast Rise		Onset of warm.  Abrupt increase in freshwater discharge: salinity drops	Century-scale, oscillations in fresh water input into the basin. Abrupt increase in freshwater discharge: salinity drops. Increase and continuous erresced condition		Glaciers retreating	1.4	v 15.8 v	21.5
	Fast Rise	Culmination of century- scale oscillations in fresh water input into the basin	Abrupt increase in freshwater discharge: salinity drops	Century-scale, oscillations in fresh water input into the basin. Abrupt increase in freshwater discharge:		Glaciers retreating	2.2	v 18.0 v	30.5
	Fast Rise	Decrease in sediment supply	Abrupt increase in freshwater discharge: salinity drops	Contundous stressed condution Century-scale, oscillations in fresh water input into the basin. Abrupt increase in freshwater discharge: salinity drops. Increase and	Progressively Increase	Alpine waxing and waning, and Apennine glaciers retreating	9.0	v 18.6 v	26
Partial collapse of the Northern Hemisphere ice sheets. Firt meltwater pulse	Rise begins (eustatic jump of 15 m)	Increase in sediment supply	Abrupt increase in freshwater discharge: salinity drops	Contury-scale, oxillations in fresh water input into the basin. Abrupt increase in freshwater discharge: salinity drops. Increase and continuous erressed continuous	Increase	Alpine and Apennine glaciers retreating	0.4	v 19.0 v	57.5
	Fall slows to stillstand	Decrease in sediment supply	Cold	Century-scale, oscillations in fresh water input into the basin. Increase and continuous stressed condition		Alpine and Apennine glaciers advancing	0.3	v 19.3 v	100
First meltwater pulse, partial collapse of N. Hemisphere ice sheets	Fall slows to stillstand	Increase in sediment supply: Onset of century- scale, oscillations in fresh water input into the basin	Cold	Onset of century-scale, oscillations in fresh water input into the basin. Increase and continuous stressed		Alpine and Apennine glaciers advancing	0.1	v 19.4 v	200
LGM Chronozone	Fall slows to stillstand	Decrease in sediment supply	Cold	Millennial oscillations in riverine input. Minor ventilation of the bottom		Alpine and Apennine glaciers	1.2	v 20.6 v	17.5
LGM Chronozone	Slower fall to 135 m below	Increase in sediment supply	Cold	Millennial oscillations in riverine input. Minor ventilation of the bottom		Alpine and Apennine glaciers	0.5	v 21.1 v	122
End of Global LGM	present sea level Slower fall to 135 m below present sea level	Decrease in sediment supply	Cold	Millennial oscillations in riverine input. Minor ventilation of the bottom		retreating Waxing and waning of Alpine and Apennine glaciers	3.1	v 24.2 v	13
Enhanced moisture source over southern Europe and Mediterranean: Global LGM	Slower fall to 135 m below present sea level	Increase in sediment supply; Composition changes: increased Ca/ Ti, K/Ti due to change in weathering intensity or location of sediment	Cold	Onset of millennial oscillations in riverine input. Minor ventilation of the bottom		Alpine and Apennine glaciers advancing	0.5	v 24.7 v	72
Greenland Stadial 3	Slower fall to 135 m below	processes in sediment supply	Relatively far from direct riverine input	Relatively well oxygenated; decreasing quality of organic matter	Progressively decreasing	Alpine and Apennine glaciers	3.7	v 28.4 v	6
Further increase in Laurentide and Scandanavian ice-sheet	Slower fall to 135 m below	Increase in sediment supply	Cold and productive			Apennine glaciers advancing	1	v 29.4 v	44
vountes Dansgaard-Oeschger Interstadial 5; Rapid growth phase of Laurentide and European ice sheets.	present sea rever Fall from 80 to 125 m below present sea level.	Overall increase in sediment supply to the basin compare to the underlaying APD succession	Cold and productive			Apennine glaciers advancing	2.4	v 31.8 v	27.5

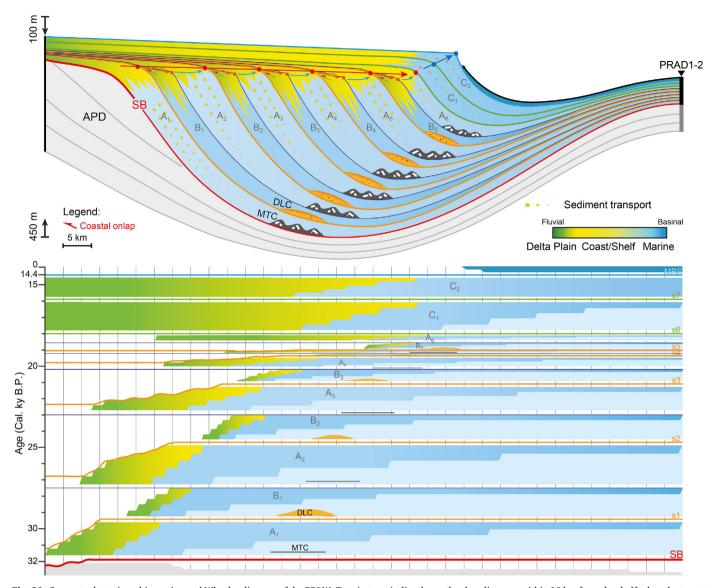


Fig. 26. Conceptual stratigraphic section and Wheeler diagram of the PRLW. Top: in type A clinothems the shoreline was within 10 km from the shelf-edge, the topset aggraded in the order of 10 m and margin destabilization was accompained by MTCs in the basin; in type B clinothems the shoreline was closer than 5 km to the shelf-edge and the topset degradation promoted the formation of DLCs; in type C clinothems the shoreline was more than 10 km landward of the shelf-edge, and coarse sediment does not reached the basin floor. Bottom: The 100's-m-high clinothems developed at centennial and millennial scale with hiatuses mostly present at the topset sector. Overall, continental facies move basinward from  $A_1$  to  $B_5$  clinothems and migrate landward from  $A_6$  to  $C_2$  clinothems (modified from Pellegrini et al., 2017a).

probably requires a grid of long cores and wells through the entire PRLW. This would enable detailed facies definition and correlation supported by refined chronological control.

#### 6. Conclusions

The stratal geometry within the Po River Lowstand Wedge, formed in 17,000 years spanning the Last Glacial Maximum, documents repeated short-term changes in accommodation and sediment supply controlling the formation of elemental shelf-edge clinothems. This revealed how the evolution of a shelf-edge system intricately convolves the influences of both global (eustacy) and regional (climate-driven supply fluctuations) controls. In particular:

Based on the available chronological control, the architectural motif
of the elemental clinothems and clinothems sets records subMilankovitch cyclicity driven by changes in fresh-water discharge;

- 2. Distinctive configurations are associated with different timing and flux of sediment delivered to the basin: respectively, i) centennial-scale, descending shelf-edge trajectory and Channel-Lobe Complexes: Type B clinothem up to 200 km³/yr; ii) millennial-scale, ascending shelf-edge trajectory and Mass Transport Complexes: Type A clinothem up to 100 km³/yr; iii) millennial-scale markedly ascending shelf-edge trajectory and mud wedges: Type C clinothem up to 30 km³/yr;
- 3. Distinctive topset geometries (type B degradational, type A moderately aggradational and type C markedly aggradational), associated with distinctive basinal deposits (respectively Channel-Lobe Complexes, Mass Transport Complexes or mud wedges), reflect subtle changes in the distance between the shoreline and the time-correlative shelf-edge that ranges from essentially zero (type B) to 10s of km (type C):
- 4. The activation and time span of channel-lobe complexes, such as within the type B clinothems can occur on the centennial scale;

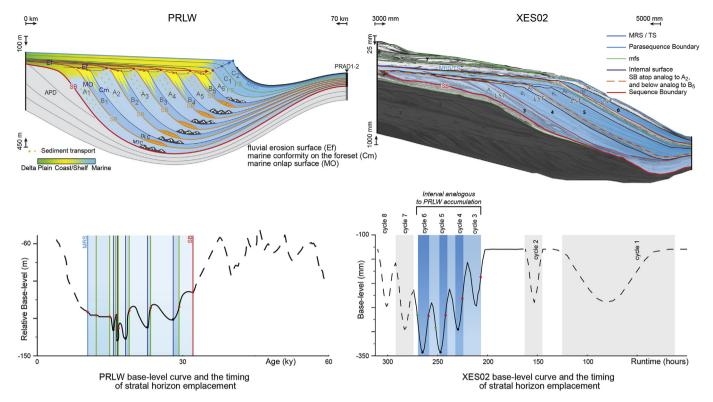


Fig. 27. Sequence stratigraphic interpretation of the PRLW as 6 high-frequency sequences overlain by 2 parasequences, based on the approaches of Mitchum et al. (1977) and Van Wagoner et al. (1990), respectively. The PRLW shows a close similarity in terms of accommodation cyclicity and stacking patterns with the XES02 experiment of Martin et al. (2009).

- 5. The progradation of Clinothem Set 1 (31.8–18.0 cal. ky BP) during eustatic fall and stillstand led to an essentially flat shelf-edge trajectory accompanied by significant sediment bypass to the basin and low-oxygen conditions at the seafloor, whereas Clinothem Set 2 (18.0–14.4 cal. ky BP) records the first phases of sea level rise through ascending shelf-edge trajectory and sediment increasingly sequestered in the topset during increasing accommodation on a broadening shelf sector, along with intermittent increases in benthic-oxygen levels;
- 6. The main sediment conduit linking the shelf to the basin occurred throughout the falling limb of the eustatic cycle (B<sub>2</sub> clinothem), but the major sediment export to the basin coincided with the lowstand when a more extensive fluvial network is established (A<sub>5</sub> clinothem);
- A substantial decoupling occurred between eustatic rise and enduring river influence on a mid-latitude continental margin impacted by post-glacial melt-water infuxes.

By recognizing the very short-time interval associated with the deposition of each elemental clinothem (few hundreds to a few thousand years) we question if, in ancient records, clinothems with a putative duration of hundreds of thousands of years might, at least in some cases, record instead much shorter intervals with most of the geological time condensed in hiatuses and stratigraphic surfaces. We suggest that the PRLW provides valuable insight into the lower end of the range of time spans recorded by such ancient margin-scale clinothems. All of these considerations reinforce the focus of classic sequence stratigraphy on surface recognition for interpretation, correlation, mapping, and prediction of rock properties. Finally, we highlighted the importance of integrating paleoenvironment data with the sequence stratigraphic method in the reconstruction of the history of a continental margin.

#### Acknowledgments

The authors dedicate this study to their colleague Giovanni Bortoluzzi, who passed away in 2015. A special tanks is due to Marco Ligi and Nevio Zitellini for geophysical data acquisition and processing; Marco Pastore and Filippo D'Oriano for their support during the cruise LSD2014 and processing of geophysical data. Elisabetta Campiani provided additional support for processing the multibeam bathymetry. A particular thank goes to Cpt. Emanuele Gentile and the crew of the R/V Urania during cruise LSD 2014. We thank Ronald Steel and an anonymous Reviewer for their constructive comments. This project was funded by ExxonMobil Upstream Research Company and by the Flagship Project RITMARE—The Italian Research for the Sea. We acknowledge the European Union Project PROMESS-1 (contract EVR1-2001-41) for borehole PRAD 1-2. This is ISMAR-CNR contribution number 1959.

#### Appendix A. Supplementary data

Supplementary data related to this article can be found at http://dx.doi.org/10.1016/j.marpetgeo.2018.03.002.

#### References

Amorosi, A., Colalongo, M.L., Fiorini, F., Fusco, F., Pasini, G., Vaiani, S.C., Sarti, G., 2004.Palaeogeographic and palaeoclimatic evolution of the Po Plain from 150-ky core records. Global Planet. Change 40 (1), 55–78.

Amorosi, A., Maselli, V., Trincardi, F., 2016. Onshore to offshore anatomy of a late Quaternary source-to-sink system (Po Plain–Adriatic Sea, Italy). Earth Sci. Rev. 153, 212–237.

Amorosi, A., Bruno, L., Campo, B., Morelli, A., Rossi, V., Scarponi, D., Hong, W., Bohacs, M.K., Drexler, T.M., 2017. Global sea-level control on local parasequence architecture from the Holocene record of the Po Plain, Italy. Mar. Petrol. Geol. 87, 99–111.

Anderson, J.B., Wallace, D.J., Simms, A.R., Rodriguez, A.B., Milliken, K.T., 2014. Variable response of coastal environments of the northwestern Gulf of Mexico to sea-level rise

- and climate change: implications for future change. Mar. Geol. 352, 348-366.
- Anderson, J.B., Wallace, D.J., Simms, A.R., Rodriguez, A.B., Weight, R.W., Taha, Z.P., 2016. Recycling sediments between source and sink during a eustatic cycle: systems of late Quaternary northwestern Gulf of Mexico Basin. Earth Sci. Rev. 153, 111–138.
- Anell, I., Midtkandal, I., 2017. The quantifiable clinothem-types, shapes and geometric relationships in the Plio-Pleistocene Giant Foresets Formation, Taranaki Basin, New Zealand. Basin Res. 29 (S1), 277–297.
- Asioli, A., 1996. High resolution foraminifera biostratigraphy in the Central Adriatic basin during the last deglaciation: a contribution to the PALICLAS Project. Memorie-Istituto Italiano di Idrobiologia 55, 197–218.
- Asioli, A., Trincardi, F., Lowe, J.J., Ariztegui, D., Langone, L., Oldfield, F., 2001. Sub-millennial scale climatic oscillations in the central Adriatic during the Late glacial: palaeoceanographic implications. Quat. Sci. Rev. 20 (11), 1201–1221.
- Asquith, D.O., 1970. Depositional topography and major marine environments, Late Cretaceous, Wyoming. AAPG (Am. Assoc. Pet. Geol.) Bull. 54 (7), 1184–1224.
- Bard, E., Hamelin, B., Arnold, M., Montaggioni, L., 1996. Deglacial sea-level record from Tahiti corals and the timing of global meltwater discharge. Nature 382 (6588), 241.
- Bard, E., Hamelin, B., Delanghe-Sabatier, D., 2010. Deglacial meltwater pulse 1B and Younger Dryas sea levels revisited with boreholes at Tahiti. Science 327 (5970), 1235–1237.
- Bazin, L., Landais, A., Lemieux-Dudon, B., Toyé Mahamadou Kele, H., Veres, D., Parrenin, F., Martinerie, P., Ritz, C., Capron, E., Lipenkov, V., Loutre, M.-F., Raynaud, D., Vinther, B., Svensson, A., Rasmussen, S.O., Severi, M., Blunier, T., Leuenberger, M., Fischer, H., Masson-Delmotte, V., Chappellaz, J., Wolff, E., 2013. An optimized multiproxy, multi-site Antarctic ice and gas orbital chronology (AICC2012): 120–800 ka. Clim. Past 9, 1715–1731.
- Beaubouef, R.T., Friedmann, S.J., 2000. High resolution seismic/sequence-stratigraphic framework for the evolution of Pleistocene intraslope basins, western Gulf of Mexico: depositional models and reservoir analogs. In: Weimer, P., Slatt, R.M., Coleman, J., Rosen, N.C., Nelson, H., Bouma, A.H., Styzen, M.J., Lawrence, D.T. (Eds.), Deepwater Reservoirs of the World: Gulf Coast Section SEPM 20th Annual Research Conference, pp. 40–60.
- Benjamin, J., Rovere, A., Fontana, A., Furlani, S., Vacchi, M., Inglis, R.H., Galili, E., Antonioli, F., Sivan, D., Miko, S., Mourtzas, N., Felja, I., Meredith-Williams, M., Goodman-Tchernov, B., Kolaiti, E., Anzidei, M., Gehrels, R., 2017. Late Quaternary sea-level changes and early human societies in the central and eastern Mediterranean Basin: an interdisciplinary review. Quat. Int. 449, 29–57.
- Bhattacharya, J.P., Copeland, P., Lawton, T.F., Holbrook, J., 2016. Estimation of source area, river paleo-discharge, paleoslope, and sediment budgets of linked deep-time depositional systems and implications for hydrocarbon potential. Earth Sci. Rev. 153, 77–110.
- Boulton, G.S., Dongelmans, P., Punkari, M., Broadgate, M., 2001. Palaeoglaciology of an ice sheet through a glacial cycle: the European ice sheet through the Weichselian. Ouat. Sci. Rev. 20 (4), 591–625.
- Bourne, A.J., Lowe, J.J., Trincardi, F., Asioli, A., Blockley, S.P.E., Wulf, S., Matthews, I.P., Piva, A., Vigliotti, L., 2010. Distal tephra record for the last ca 105,000 years from core PRAD 1-2 in the central Adriatic Sea: implications for marine tephrostratigraphy. Quat. Sci. Rev. 29, 3079–3094.
- Boyd, R., Suter, J., Penland, S., 1989. Relation of sequence stratigraphy to modern sedimentary environments. Geology 17 (10), 926–929.
- Bruno, L., Amorosi, A., Severi, P., Costagli, B., 2017. Late Quaternary aggradation rates and stratigraphic architecture of the southern Po Plain, Italy. Basin Res. 29 (2), 234–248
- Burgess, P.M., Prince, G.D., 2015. Non-unique stratal geometries: implications for sequence stratigraphic interpretations. Basin Res. 27 (3), 351–365.
- Calanchi, N., Dinelli, E., 2008. Tephrostratigraphy of the last 170 ka in sedimentary successions from the Adriatic Sea. J. Volcanol. Geoth. Res. 177 (1), 81–95.
- Calves, G., Toucanne, S., Jouet, G., Charrier, S., Thereau, E., Etoubleau, J., Marseset, T., Droz, L., Bez, M., Abreu, V., Jorry, S., Mulder, T., Lericolais, G., 2013. Inferring denudation variations from the sediment record; an example of the last glacial cycle record of the Golo Basin and watershed, East Corsica, western Mediterranean sea. Basin Res. 25 (2), 197–218.
- Campo, B., Amorosi, A., Vaiani, S.C., 2017. Sequence stratigraphy and late Quaternary paleoenvironmental evolution of the Northern Adriatic coastal plain (Italy). Palaeogeogr. Palaeoclimatol. Palaeoecol. 466, 265–278.
- Carlson, A.E., Clark, P.U., 2012. Ice sheet sources of sea level rise and freshwater discharge during the last deglaciation. Rev. Geophys. 50 (4), 1–72.
- Carvajal, C.R., Steel, R.J., 2006. Thick turbidite successions from supply-dominated shelves during sea-level highstand. Geology 34 (8), 665–668.
- Carvajal, C., Steel, R., Petter, A., 2009. Sediment supply: the main driver of shelf-margin growth. Earth Sci. Rev. 96 (4), 221–248.
- Cattaneo, A., Correggiari, A., Langone, L., Trincardi, F., 2003. The late-Holocene Gargano subaqueous delta, Adriatic shelf: sediment pathways and supply fluctuations. Mar. Geol. 193 (1), 61–91.
- Catuneanu, O., Abreu, V., Bhattacharya, J.P., Blum, M.D., Dalrymple, R.W., Eriksson, P.G., Winker, C., 2009. Towards the standardization of sequence stratigraphy. Earth Sci. Rev. 92 (1), 1–33.
- Chappell, J., Shackleton, N.J., 1986. Oxygen isotopes and sea level. Nature 324, 137–140. http://dx.doi.org/10.1038/324137a0.
- Clark, P.U., McCabe, A.M., Mix, A.C., Weaver, A.J., 2004. Rapid rise of sea level 19,000 years ago and its global implications. Science 304 (5674), 1141–1144.
- Dyke, A.S., Andrews, J.T., Clark, P.U., England, J.H., Miller, G.H., Shaw, J., Veillette, J.J., 2002. The Laurentide and Innuitian ice sheets during the last glacial maximum. Quat. Sci. Rev. 21 (1), 9–31.
- Dalla Valle, G., Gamberi, F., Trincardi, F., Baglioni, L., Errera, A., Rocchini, P., 2013.Contrasting slope channel styles on a prograding mud-prone margin. Mar. Petrol.

- Geol. 41, 72-82.
- Doglioni, C., Mongelli, F., Pieri, P., 1994. The Puglia uplift (SE Italy): an anomaly in the foreland of the Apenninic subduction due to buckling of a thick continental lithosphere. Tectonics 13, 1309–1321. http://dx.doi.org/10.1029/94TC01501.
- Donnici, S., Serandrei Barbero, R., Taroni, G., 1997. Living benthic foraminifera in the lagoon of Venice (Italy): population dynamics and its significance. Micropaleontology 43, 440–454.
- Eberli, G.P., Anselmetti, F.S., Kroon, D., Sato, T., Wright, J.D., 2002. The chronostratigraphic significance of seismic reflections along the Bahamas Transect. Mar. Geol. 185 (1), 1–17.
- Embry, A.F., Johannessen, E.P., 2017. Two approaches to sequence stratigraphy. In Stratigraphy & Timescales 2, 85–118. http://dx.doi.org/10.1016/bs.sats.2017.08. 001
- Fairbanks, R.G., 1989. A 17, 000-year glacio-eustatic sea level record: influence of glacial melting rates on the Younger Dryas event and deep-ocean circulation. Nature 342 (6250), 637–642.
- Fanget, A.S., Berné, S., Jouet, G., Bassetti, M.A., Dennielou, B., Maillet, G.M., Tondut, M., 2014. Impact of relative sea level and rapid climate changes on the architecture and lithofacies of the Holocene Rhone subaqueous delta (Western Mediterranean Sea). Sediment. Geol. 305, 35–53.
- Fatoke, O.A., Bhattacharya, J.P., 2010. Controls on depositional systems and sequence stratigraphy of the Pliocene-Pleistocene strata of eastern Niger delta, Nigeria. Search and Discovery Article 10220.
- Florineth, D., Schlüchter, C., 1998. Reconstructing the last glacial maximum (LGM) ice surface geometry and flowlines in the central Swiss Alps. Eclogae Geol. Helv. 91, 391–407
- Frignani, M., Langone, L., Ravaioli, M., Sorgente, D., Alvisi, F., Albertazzi, S., 2005. Fine-sediment mass balance in the western Adriatic continental shelf over a century time scale. Mar. Geol. 222, 113–133.
- Geletti, R., Del Ben, A., Busetti, M., Ramella, R., Volpi, V., 2008. Gas seeps linked to salt structures in the Central Adriatic Sea. Basin Res. 20 (4), 473–487.
- Ghielmi, M., Minervini, M., Nini, C., Rogledi, S., Rossi, M., 2013. Late Miocene–Middle Pleistocene sequences in the Po Plain–Northern Adriatic Sea (Italy): the stratigraphic record of modification phases affecting a complex foreland basin. Mar. Petrol. Geol. 42, 50–81
- Giraudi, C., 2017. Climate evolution and forcing during the last 40 ka from the oscillations in Apennine glaciers and high mountain lakes, Italy. J. Quat. Sci. 32 (8), 1085–1098.
- Goineau, A., Fontanier, C., Jorissen, F.J., Lansard, B., Buscail, R., Mouret, A., Kerhervé, P., Zaragosi, S., Ernoult, E., Artéro, C., Anschutz, P., Metzger, E., Rabouill, C., 2011. Live (stained) benthic foraminifera from the Rhône prodelta (Gulf of Lion, NW Mediterranean): environmental controls on a river-dominated shelf. J. Sea Res. 65, 58–75.
- Gong, C., Steel, R.J., Wang, Y., Lin, C., Olariu, C., 2016. Shelf-margin architecture variability and its role in sediment-budget partitioning into deep-water areas. Earth Sci. Rev. 154, 72–101.
- Hayward, W., Kawagata, S., Sabaa, A., Grenfell, H., Van Kerckhoven, L., Johnson, K., Thomas, E., 2012. The Last Global Extinction (Mid-pleistocene) of Deep-sea Benthic Foraminifera (Chrysalogoniidae, Ellipsoidinidae, Glandulonodosariidae, Plectofrondiculariidae, Pleurostomellidae, Stilostomellidae), Their Late Cretaceouscenozoic History and Taxonomy. vol. 43. Cushman Foundation for Foraminiferal Research Special Publication, pp. 408.
- Helland-Hansen, W., Martinsen, O.J., 1996. Shoreline trajectories and sequences: description of variable depositional-dip scenarios. J. Sediment. Res. 66 (4), 670–688.
- Helland-Hansen, W., Hampson, G.J., 2009. Trajectory analysis: concepts and applications. Basin Res. 21 (5), 454–483.
- Hemleben, C., Spindler, M., Anderson, O.R., 1989. Modern Planktonic Foraminifera. Springer-Verlag, New York, pp. 1–363.
- Henriksen, S., Hampson, G.J., Helland-Hansen, W., Johannessen, E.P., Steel, R.J., 2009. Shelf edge and shoreline trajectories, a dynamic approach to stratigraphic analysis. Basin Res. 21 (5), 445–453.
- Hess, S., Jorissen, F.J., 2009. Distribution patterns of living benthic foraminifera from Cap Breton canyon, Bay of Biscay: faunal response to sediment instability. Deep Sea Res., Part I 56, 1555–1578. http://dx.doi.org/10.1016/j.dsr.2009.04.003.
- Hodgson, D.M., Browning, J.V., Miller, K.G., Hesselbo, S.P., Poyatos-Moré, M., Mountain, G.S., Proust, J.N., 2018. Sedimentology, stratigraphic context, and implications of Miocene intrashelf bottomset deposits, offshore New Jersey. Geosphere 14 (1), 95–114.
- Hohenegger, J., Piller, W., Baal, Ch, 1989. Reasons for the spatial microdistributions of foraminifers in an intertidal pool (Northern Adriatic Sea). P.S.Z.N. I. Marine Ecology 10, 43–78 (Berlin-Hamburg).
- Hovland, M., Curzi, P., 1989. Gas seepage and assumed mud diapirism in the Italian central Adriatic Sea. Mar. Petrol. Geol. 6, 161–169.
- Hughes, P.D., Gibbard, P.L., 2015. A stratigraphical basis for the last glacial maximum (LGM). Quat. Int. 383, 174–185.
- IEA, 2013. Resources to Reserves 2013: Oil, Gas, and Coal Technologies for Energy Markets of the Future. OECD-IEA, Paris, France, 978-92-64-08354-7pp. 272.
- Jerolmack, D.J., Paola, C., 2010. Shredding of environmental signals by sediment transport. Geophys. Res. Lett. 37 (19).
- Jervey, M.T., 1988. Quantitative geological modeling of siliciclastic rock sequences and their seismic expression. In: In: Wilgus, C.K., Hastings, B.S., Kendall, C.G.St.C., Posamentier, H.W., Ross, C.A., Van Wagoner, J.C. (Eds.), Sea Level Changes — An Integrated Approach. Special Publication, vol. 42. Society of Economic Paleontologists and Mineralogists (SEPM), pp. 47–69.
- Johannessen, E.P., Steel, R.J., 2005. Shelf-margin clinoforms and prediction of deepwater sands. Basin Res. 17 (4), 521–550.

- Jorissen, F.J., 1987. The distribution of benthic foraminifera in the Adriatic Sea. Mar. Micropaleontol. 12, 21–48.
- Jorissen, F.J., 1988. Benthic foraminifera from the Adriatic Sea; principles of phenotypic variation. Utrecht Micropaleontol. Bull. 37, 176.
- Jorissen, F.J., Asioli, A., Borsetti, A., Capotondi, L., De Visser, J., Hilgen, F., Rohling, E., Van der Borg, K., Grazzini, C.V., Zachariasse, W., 1993. Late quaternary central Mediterranean biochronology. Mar. Micropaleontol. 21, 169–189.
- Jorissen, F.J., 1999. Benthic foraminiferal successions across late quaternary mediterranean sapropels. Mar. Geol. 153, 91–101.
- Kettner, A.J., Syvitski, J.P., 2008. HydroTrend v. 3.0: a climate-driven hydrological transport model that simulates discharge and sediment load leaving a river system. Comput. Geosci. 34 (10), 1170–1183.
- Klausen, T.G., Ryseth, A.E., Helland-Hansen, W., Gawthorpe, R., Laursen, I., 2015.Regional development and sequence stratigraphy of the middle to late triassic snadd formation, Norwegian barents sea. Mar. Petrol. Geol. 62, 102–122.
- Knudsen, K.L., 1971. Late quaternary foraminifera from the vendsyssel, Denmark and sandnes, Norway - systematic part. In: In: Knudsen, K.L., Feyling-hanssen, Jørgensen, Knudsen, Lykke Andersen (Eds.), Late Quaternary Foraminifera from the Vendsyssel, Denmark and Sandnes, Norway, vol. 21. Bulletin of the Geological Society of Denmark, pp. 185–295.
- Lambeck, K., Rouby, H., Purcell, A., Sun, Y., Sambridge, M., 2014. sea level and global ice volumes from the last glacial maximum to the holocene. Proc. Natl. Acad. Sci. Unit. States Am. 111 (43), 15296–15303.
- Lea, D.W., Martin, P.A., Pak, D.K., Spero, H.J., 2002. Reconstructing a 350ky history of sea level using planktonic Mg/Ca and oxygen isotope records from a Cocos Ridge core. Quat. Sci. Rev. 21 (1), 283–293.
- Madof, A.S., Harris, A.D., Connell, S.D., 2016. Nearshore along-strike variability: is the concept of the systems tract unhinged? Geology 44 (4), 315–318.
- Madof, A.S., Christie-Blick, N., Anders, M.H., Febo, L.A., 2017. Unreciprocated sedimentation along a mud-dominated continental margin, Gulf of Mexico, USA: implications for sequence stratigraphy in muddy settings devoid of depositional sequences. Mar. Petrol. Geol. 80, 492–516.
- Mallarino, G., Beaubouef, R.T., Droxler, A.W., Abreu, V., Labeyrie, L., 2006. Sea level influence on the nature and timing of a minibasin sedimentary fill (northwestern slope of the Gulf of Mexico). AAPG Bull. 90 (7), 1089–1119.
- Martin, J., Paola, C., Abreu, V., Neal, J., Sheets, B., 2009. Sequence stratigraphy of experimental strata under known conditions of differential subsidence and variable base level. AAPG Bull. 93 (4), 503–533.
- Maselli, V., Trincardi, F., Cattaneo, A., Ridente, D., Asioli, A., 2010. Subsidence patterns in the central Adriatic and its influence on sediment architecture during the last 400 kyr. J. Geophys. Res.: Solid Earth 115 (B12). http://dx.doi.org/10.1029/ 2010JB007687.
- Milliman, J.D., Farnsworth, K.L., 2013. River discharge to the coastal ocean: a global synthesis. Global Planet. Change 39, 53–64.
- Milliman, J.D., Bonaldo, D., Carniel, S., 2016. Flux and fate of river-discharged sediments to the Adriatic Sea. Adv. Oceanogr. Limnol. 7 (2).
- Minisini, D., Eldrett, J., Bergman, S.C., Forkner, R., 2017. Chronostratigraphic framework and depositional environments in the organic-rich, mudstone-dominated Eagle Ford Group, Texas, USA. Sedimentology. http://dx.doi.org/10.1111/sed.12437.
- Mitchum Jr., R.M., Vail, P.R., Sangree, J.B., 1977. Seismic stratigraphy and global changes of sea level: Part 6. Stratigraphic interpretation of seismic reflection patterns in depositional sequences: section 2. Application of seismic reflection configuration to stratigraphic interpretation.
- Mitchum, R.M.J., Van Wagoner, J.C., 1991. High-frequency sequences and their stacking patterns: sequence-stratigraphic evidence of high-frequency eustatic cycles. Sediment. Geol. 70 (2–4), 131–160. http://dx.doi.org/10.1016/0037-0738(91) 90139-5.
- Mitrovica, J.X., 2003. Recent controversies in predicting post-glacial sea-level change. Quat. Sci. Rev. 22 (2), 127–133.
- Mojtahid, M., Jorissen, F., Lansard, B., Fontanier, C., Bombled, B., Rabouille, C., 2009. Spatial distribution of live benthic foraminifera in the Rhône prodelta: faunal response to a continental-marine organic matter gradient. Mar. Micropaleontol. 70 (3–4), 177–200.
- Monegato, G., Ravazzi, C., Donegana, M., Pini, R., Calderoni, G., Wick, L., 2007. Evidence of a two-fold glacial advance during the last glacial maximum in the Tagliamento end moraine system (eastern Alps). Quat. Res. 68, 284–302. http://dx.doi.org/10.1016/j. vqres.2007.07.002.
- Monegato, G., Scardia, G., Hajdas, I., Rizzini, F., Piccin, A., 2017. The Alpine LGM in the boreal icesheets game. Sci. Rep. 7 (2078). http://dx.doi.org/10.1038/s41598-017-02148-7.
- Mulder, T., Syvitski, J.P.M., 1995. Turbidity currents generated at river mouths during exceptional discharges to the world oceans. J. Geol. 103, 285–299.
- Muller-Karger, F.E., Varela, R., Thunell, R., Luerssen, R., Hu, Chuanamin, Walsh, J.J., 2005. The importance of continental margins in the global carbon cycle. Geophys. Res. Lett. 32, L01602.
- Murray, J.W., 2006. Ecology and Applications of Benthic Foraminifera. Cambridge University Press, pp. 426.
- Murray, J.W., 2013. Living benthic foraminifera: biogeographical distributions and the significance of rare morphospecies. J. Micropalaeontol. 32, 1–58.
- Muto, T., Steel, R.J., 1997. Principles of regression and transgression: the nature of the interplay between accommodation and sediment supply: perspectives. J. Sediment. Res. 67 (6).
- Neal, J., Abreu, V., 2009. Sequence stratigraphy hierarchy and the accommodation succession method. Geology 37 (9), 779–782.
- Neal, J.E., Abreu, V., Bohacs, K.M., Feldman, H.R., Pederson, K.H., 2016. Accommodation succession ( $\delta A/\delta S$ ) sequence stratigraphy: observational method, utility and insights

- into sequence boundary formation. J. Geol. Soc. 173 (5), 803-816.
- Olariu, C., Bhattacharya, J.P., 2006. Terminal distributary channels and delta front architecture of river-dominated delta systems. J. Sediment. Res. 76 (2), 212–233.
- Patruno, S., Hampson, G.J., Jackson, C.A., 2015. Quantitative characterisation of deltaic and subaqueous clinoforms. Earth Sci. Rev. 142, 79–119.
- Pellegrini, C., Maselli, V., Cattaneo, A., Piva, A., Ceregato, A., Trincardi, F., 2015. Anatomy of a compound delta from the post-glacial transgressive record in the Adriatic Sea. Mar. Geol. 362, 43–59.
- Pellegrini, C., Maselli, V., Trincardi, F., 2016. Pliocene–Quaternary contourite depositional system along the south-western Adriatic margin: changes in sedimentary stacking pattern and associated bottom currents. Geo Mar. Lett. 36 (1), 67–79.
- Pellegrini, C., Maselli, V., Gamberi, F., Asioli, A., Bohacs, K.M., Drexler, T.M., Trincardi, F., 2017a. How to make a 350-m-thick lowstand systems tract in 17,000 years: the Late Pleistocene Po River (Italy) lowstand wedge. Geology 45, 327–330.
- Pellegrini, C., Bohacs, K.M., Drexler, T.M., Gamberi, F., Rovere, M., Trincardi, F., 2017b. Identifying the sequence boundary in over- and under-supplied contexts: the case of the late Pleistocene adriatic continental margin. In: Hart, B., Rosen, N.C., West, D., D'Agostino, A., Messina, C., Hoffman, M., Wild, R. (Eds.), Sequence Stratigraphy: the Future Defined, Proceedings of the 36th Annual Perkins-Rosen Research Conference; 2017. GCSSEPM Foundation, Houston, Texas, pp. 160–182. https://doi.org/10.5724/gcs.17.36.160.
- Peltier, W.R., Fairbanks, R.G., 2006. Global glacial ice volume and Last Glacial Maximum duration from an extended Barbados sea level record. Quat. Sci. Rev. 25 (23), 3322–3337.
- Peng, Y., Steel, R.J., Rossi, V.M., Olariu, C., 2018. Mixed-energy process interactions read from a compound-clinoform delta (paleo–Orinoco Delta, Trinidad): preservation of river and tide signals by mud-induced wave damping. J. Sediment. Res. 88 (1), 75–90.
- Pillans, B., Chappell, J., Naish, T.R., 1998. A review of the Milankovitch climatic beat: template for Plio–Pleistocene sea-level changes and sequence stratigraphy. Sediment. Geol. 122 (1), 5–21.
- Pirmez, C., Pratson, L.F., Steckler, M.S., 1998. Clinoform development by advection-diffusion of suspended sediment: modeling and comparison to natural systems. J. Geophys. Res.: Solid Earth (1978–2012) 103 (B10), 24141–24157.
- Piva, A., Asioli, A., Schneider, R.R., Trincardi, F., Andersen, N., Colmenero-Hidalgo, E., Dennielou, B., Flores, J.A., Vigliotti, L., 2008a. Climatic cycles as expressed in sediments of the PROMESSI borehole PRAD1-2, Central Adriatic, for the last 370 ka, 1: integrated stratigraphy. G-cubed 9 (1), Q01R01. http://dx.doi.org/10.1029/ 2007GC001713.
- Piva, A., Asioli, A., Andersen, N., Grimalt, J.O., Schneider, R.R., Trincardi, F., 2008b. Climatic cycles as expressed in sediments of the PROMESS1 borehole PRAD1-2, central Adriatic, for the last 370 ka: 2. Paleoenvironmental evolution. G-cubed 9 (3).
- Plink-Björklund, P., Mellere, D., Steel, R.J., 2001. Turbidite variability and architecture of sand-prone, deep-water slopes: eocene clinoforms in the Central Basin, Spitsbergen. J. Sediment. Res. 71 (6), 895–912.
- Plint, A.G., Kreitner, M.A., 2007. Extensive thin sequences spanning Cretaceous foredeep suggest high-frequency eustatic control: late Cenomanian, Western Canada foreland basin. Geology 35 (8), 735–738.
- Porębski, S.J., Steel, R.J., 2003. Shelf-margin deltas: their stratigraphic significance and relation to deepwater sands. Earth Sci. Rev. 62 (3), 283–326.
- Poyatos-Moré, M., Jones, G.D., Brunt, R.L., Hodgson, D.M., Wild, R.J., Flint, S.S., 2016. Mud-dominated basin-margin progradation: processes and implications. J. Sediment. Res. 86 (8), 863–878.
- Prather, B.E., Booth, J.R., Steffens, G.S., Craig, P.A., 1998. Classification, lithologic calibration, and stratigraphic succession of seismic facies of intraslope basins, deepwater Gulf of Mexico. AAPG Bull. 82 (5), 701–728.
- Pujol, C., Vergnaud-Grazzini, C., 1995. Distribution patterns of live planktic foraminifera as related to regional hydrography and productive systems of the Mediterranean Sea. Mar. Micropaleontol. 25, 187–217.
- Ramon-Duenas, C., Rudolph, K.W., Emmet, P.A., Wellner, J.S., 2018. Quantitative analysis of siliciclastic clinoforms: an example from the North Slope, Alaska. Mar. Petrol. Geol.
- Ridente, D., Trincardi, F., Piva, A., Asioli, A., 2009. The combined effect of sea level and supply during Milankovitch cyclicity: evidence from shallow-marine  $\delta 180$  records and sequence architecture (Adriatic margin). Geology 37, 1003–1006.
- Roberts, H.H., Fillon, R.H., Kohl, B., Robalin, J.M., Sydow, J.C., 2004. Depositional Architecture of the Lagniappe Delta: Sediment Characteristics, Timing of Depositional Events, and Temporal Relationship with Adjacent Shelf-edge Deltas.
- Rossi, M., Minervini, M., Ghielmi, M., Rogledi, S., 2015. Messinian and Pliocene erosional surfaces in the Po Plain-Adriatic Basin: insights from allostratigraphy and sequence stratigraphy in assessing play concepts related to accommodation and gateway turnarounds in tectonically active margins. Mar. Petrol. Geol. 66, 192–216.
- Royden, L., Patacca, E., Scandone, P., 1987. Segmentation and configuration of subducted lithosphere in Italy: an important control on thrust-belt and foredeep-basin evolution. Geology 15 (8), 714–717.
- Ryan, M.C., Helland-Hansen, W., Johannessen, E.P., Steel, R.J., 2009. Erosional vs. accretionary shelf margins: the influence of margin type on deepwater sedimentation: an example from the Porcupine Basin, offshore western Ireland. Basin Res. 21 (5), 676–703.
- Schmiedl, G., de Bovèe, F., Buscail, R., Charrière, B., Hemleben, C., Medernach, L., Picon, P., 2000. Trophic control of benthic foraminiferal abundance and microhabitat in the bathyal Gulf of Lions, western Mediterranean Sea. Mar. Micropaleontol. 40, 167–188.
- Shanley, K.W., McCabe, P.J., 1991. Predicting facies architecture through sequence stratigraphy—an example from the Kaiparowits Plateau, Utah. Geology 19 (7), 742–745.
- Siddall, M., Rohling, E.J., Almogi-Labin, A., Hemleben, C., Meischner, D., Schmelzer, I.,

- Smeed, D.A., 2003. Sea-level fluctuations during the last glacial cycle. Nature 423 (6942), 853–858.
- Simeoni, U., Pano, N., Ciavola, P., 1997. The coastline of Albania: morphology, evolution and coastal management issues. CIESM Publ. 18 561–168.
- Steckler, M.S., Mountain, G.S., Miller, K.G., Christie-Blick, N., 1999. Reconstruction of Tertiary progradation and clinoform development on the New Jersey passive margin by 2-D backstripping. Mar. Geol. 154, 399–420.
- Steel, R.J., Crabaugh, J., Schellpeper, M., Mellere, D., Plink-Björklund, P., Deibert, J., Loeseth, T., 2000. Deltas vs. rivers on the shelf edge: their relative contributions to the growth of shelf-margins and basin-floor fans (Barremian and Eocene, Spitsbergen). Deepwater Reservoirs of the World, 981–1009.
- Storms, J.E., Weltje, G.J., Terra, G.J., Cattaneo, A., Trincardi, F., 2008. Coastal dynamics under conditions of rapid sea-level rise: late Pleistocene to Early Holocene evolution of barrier–lagoon systems on the northern Adriatic shelf (Italy). Quat. Sci. Rev. 27 (11), 1107–1123.
- Suter, J.R., Berryhill Jr., H.L., 1985. Late Quaternary shelf-margin deltas, northwest Gulf of Mexico. AAPG (Am. Assoc. Pet. Geol.) Bull. 69 (1), 77–91.
- Sydow, J., Finneran, J., Bowman, A.P., Rosen, H., Fillon, R., Anderson, J., 2003. Stacked shelf-edge delta reservoirs of the columbus basin, trinidad, west indies. Shelf-Margin Deltas and Linked Downslope Petroleum Systems 441–465.
- Sweet, M.L., Blum, M.D., 2016. Connections between fluvial to shallow marine environments and submarine canyons: implications for sediment transfer to deep water. J. Sediment. Res. 86 (10), 1147–1162.
- Sweetman, A.K., Sommer, S., Pfannkuche, O., Witte, U., 2009. Retarded response by macrofauna-size foraminifera to phytodetritus in a deep Norwegian fjord. J. Foraminifer. Res. 39 (1), 15–22.
- Swenson, J.B., Paola, C., Pratson, L., Voller, V.R., Murray, A.B., 2005. Fluvial and marine controls on combined subaerial and subaqueous delta progradation: morphodynamic modeling of compound-clinoform development. J. Geophys. Res.: Earth Surface 110, 0148–0227.
- Tarasov, L., Peltier, W.R., 2004. A geophysically constrained large ensemble analysis of the deglacial history of the North American ice-sheet complex. Quat. Sci. Rev. 23 (3), 359–388.
- Tesi, T., Asioli, A., Minisini, D., Maselli, V., Dalla Valle, G., Gamberi, F., Langone, L., Cattaneo, A., Montagna, P., Trincardi, F., 2017. Large-scale response of the Eastern Mediterranean thermohaline circulation to African monsoon intensification during sapropel S1 formation. Ouat. Sci. Rev. 159, 139–154.
- Trincardi, F., Field, M.E., 1991. Geometry, lateral variation, and preservation of downlapping regressive shelf deposits: eastern Tyrrhenian Sea margin, Italy. J. Sediment. Res. 61 (5).
- Trincardi, F., Correggiari, A., Roveri, M., 1994. Late Quaternary transgressive erosion and deposition in a modern epicontinental shelf: the Adriatic semienclosed basin. Geo Mar. Lett. 14 (1), 41–51.
- Trincardi, F., Cattaneo, A., Asioli, A., Correggiari, A., Langone, L., 1996. Stratigraphy of the late-Quaternary deposits in the central Adriatic basin and the record of short-term

- climatic events. In: Oldfield, F., Guilizzoni, P. (Eds.), Palaeoenvironmental Analysis of Italian Crater Lake and Adriatic Sediments. Memorie dell'Istituto Italiano di Idrobiologia. vol. 55. pp. 39–70.
- Trincardi, F., Correggiari, A., 2000. Quaternary Forced Regression Deposits in the Adriatic Basin and the Record of Composite Sea-level Cycles. Geological Society 172 (1), 245–269 London, Special Publications.
- Trincardi, F., Cattaneo, A., Correggiari, A., Ridente, D., 2004. Evidence of soft sediment deformation, fluid escape, sediment failure and regional weak layers within the late Quaternary mud deposits of the Adriatic Sea. Mar. Geol. 213 (1), 91–119.
- Urgeles, R., Cattaneo, A., Puig, P., Liquete, C., De Mol, B., Amblàs, D., Trincardi, F., 2011. A review of undulated sediment features on Mediterranean prodeltas: distinguishing sediment transport structures from sediment deformation. Mar. Geophys. Res. 32 (1–2), 49–69.
- Vail, P.R., Mitchum Jr., R.M., Thompson III, S., 1977. Seismic stratigraphy and global changes of sea level: Part 4. Global cycles of relative changes of sea level: section 2. Application of Seismic Reflection Configuration to Stratigraphic Interpretation.
- Vail, P.R., Audemard, F., Bowman, S.A., Eisner, P.N., Perez-Cruz, G., 1991. The stratigraphic signatures of tectonics, eustasy and sedimentation: an overview. In: Seilacher, A., Eisner, G. (Eds.), Cycles and Events in Stratigraphy. Springer-Verlag, Tiibingen, pp. 617–659.
- Van der Zwaan, G.J., Jorissen, F.J., 1991. Biofacial patterns in river –induced anoxia. In: In: Tyson, R., Pearson, Th (Eds.), Modern and Ancient Continental Shelf Anoxia, vol. 58. Geological Society of London Special Publication, pp. 65–82.
- Van Wagoner, J.C., Mitchum, R.M., Campion, K.M., Rahmanian, V.D., 1990. Siliciclastic Sequence Stratigraphy in Well Logs, Cores, and Outcrops: Concepts for High-resolution Correlation of Time and Facies.
- Walker, M.J.C., Berkelhammer, M., Björck, S., Cwynar, L.C., Fisher, D.A., Long, A.J., Lowe, J.J., Newnham, R.M., Rasmussen, S.O., Weiss, H., 2009. Formal subdivision of the holocene series/epoch: a discussion paper by a working group of intimate (integration of ice-core, marine and terrestrial records) and the subcommission on quaternary stratigraphy (international commission on stratigraphy). J. Quat. Sci. 27 (7), 649–659.
- Walsh, J.J., 1991. Importance of continental margins in the marine biogeochemical cycling of carbon and nitrogen. Nature 350, 53–55. http://dx.doi.org/10.1038/350053a0.
- Wellner, J.S., Sarzalejo, S., Lagoe, M., Anderson, J.B., 2004. Late Quaternary Stratigraphic Evolution of the West Louisiana/east Texas Continental Shelf. SEPM Special Publication No. 79, pp. 217–235.
- Yokoyama, Y., Lambeck, K., De Deckker, P., Johnston, P., Fifield, L.K., 2000. Timing of the last glacial maximum from observed sea-level minima. Nature 406 (6797), 713–716.
- Zecchin, M., Baradello, L., Brancolini, G., Donda, F., Rizzetto, F., Tosi, L., 2008. Sequence stratigraphy based on high-resolution seismic profiles in the late Pleistocene and Holocene deposits of the Venice area. Mar. Geol. 253 (3), 185–198.